



Clumped isotope thermometry reveals diagenetic origin of the dolomite layer within late Ordovician black shale of the Guanyinqiao Bed (SW China)

Xiaolong Hu^{a,b,c}, Inigo A. Müller^c, Ankun Zhao^d, Martin Ziegler^c, Qing Chen^e, Lu Han^{a,b}, Zhiqiang Shi^{a,b,*}

^a State Key Laboratory of Oil and Gas Reservoir Geology and Exploitation, Chengdu University of Technology, Chengdu, Sichuan 610059, China

^b Institute of Sedimentary Geology, Chengdu University of Technology, Chengdu, Sichuan 610059, China

^c Department of Earth Sciences, Faculty of Geosciences, Utrecht University, Utrecht 3584 CB, the Netherlands

^d Chengdu Geological Survey Center, China Geological Survey, Chengdu, Sichuan 610081, China

^e State Key Laboratory of Palaeobiology and Stratigraphy, Nanjing Institute of Geology and Palaeontology, Chinese Academy of Science, Nanjing, Jiangsu 210008, China

ARTICLE INFO

Editor: Dr Claudia Romano

Keywords:

Late Ordovician
Guanyinqiao Bed
Organic-rich dolomite
Geochemistry
Clumped isotope thermometry

ABSTRACT

The origin of widespread dolomite deposits in Paleozoic strata is a longstanding open question. Here we use a suite of geochemical methods to investigate a prominent Paleozoic dolomite occurrence in SW China. The upper Ordovician Wufeng Formation of the upper Yangtze Block (SW China) covers the time interval just before the Ordovician-Silurian Mass Extinction event, consisting of wide-spread black shale with an interlayer of bioclastic limestone, the Guanyinqiao Bed. In the western part of the Yangtze Block, in Shizhu county however, the Guanyinqiao Bed contains a particular organic-rich dolomite interlayer of which the formation mechanism is unclear. To distinguish between potential primary dolomite precipitation and late stage diagenetic/magmatic alteration, we studied this dolomite interlayer with petrological and geochemical techniques including microscopy, REE content and carbonate clumped isotope thermometry.

The petrological observations show micritic dolomite with euhedral-subhedral shape and relatively low ordering (0.33 to 0.39). Conventional stable isotope analysis revealed negative carbon ($\delta^{13}\text{C}$ of $-3.17 \pm 0.04\text{‰}$ to $-2.48 \pm 0.03\text{‰}$) and oxygen isotope compositions ($\delta^{18}\text{O}$ of $-11.28 \pm 0.18\text{‰}$ to $-10.99 \pm 0.20\text{‰}$), and the organic carbon content ranged from 3.69% to 4.33%. The averaged clumped isotope temperature estimate revealed hot dolomite formation conditions of 87_{-10}^{+11} °C, in a presumable fluid source with isotopic composition of $\delta^{18}\text{O}_w = -1.8_{-1.5}^{+1.5}\text{‰}$. The elevated formation temperature estimates, the slightly depleted $\delta^{18}\text{O}$ of dolomite ($\sim -11.14\text{‰}$) with respect to contemporary deposited limestone ($\sim -10\text{‰}$) and the $\delta^{18}\text{O}_w$ which is similar to the assumed late Ordovician seawater points at diagenetic alteration of primary limestone at a burial depth of approximately 3000 m. The analyzed dolomite samples with low contents of Fe, Zn and small Eu anomaly show further evidence for a diagenetic fluid source and exclude magmatic/hydrothermal alteration. We suggest that at this burial depth the temperature pressure conditions triggered significant Mg release from the surrounding clay to the diagenetic fluid, providing ideal conditions to transform the primary limestone into diagenetic dolomite.

1. Introduction

Dolomite deposits have a widespread occurrence in Paleozoic successions, and they often occur in association with black shales. Dolomite layers in shale were observed and studied in Permian lacustrine

sediments of Lucaogou Formation (Lei et al., 2012; Liu et al., 2019; Wang et al., 2017b; Zhang, 1993) and Silesian Basin in south Poland of Eocene to Oligocene (Bojanowski, 2014). Several studies suggest that dolomite found in shales is associated with methanogenesis and bacterial activity. However, other studies point at a diagenetic origin, such as

* Corresponding author at: State Key Laboratory of Oil and Gas Reservoir Geology and Exploitation, Chengdu University of Technology, Chengdu, Sichuan 610059, China.

E-mail address: szqcdut@163.com (Z. Shi).

<https://doi.org/10.1016/j.chemgeo.2021.120641>

Received 18 May 2021; Received in revised form 8 November 2021; Accepted 18 November 2021

Available online 25 November 2021

0009-2541/© 2021 Elsevier B.V. All rights reserved.

Phan et al. (2019) on dolomite found in Marcellus shale at Monongalia county (USA) of the middle Devonian. Besides, dolomite in black shale is also found in the Precambrian Doushantuo Formation (Gao et al., 2020; Lan et al., 2019; Ostrander et al., 2019; Wu et al., 2019; Wang et al., 2017a). Previous studies have however focused on aspects of this succession such as the origin of chert nodules (Gao et al., 2020), chemostratigraphic correlation (Lan et al., 2019), the excursion of Mo isotope to interpret the global ocean redox changes (Ostrander et al., 2019), the positive anomaly of Ce isotope (Wu et al., 2019) and silicified glendonites to reveal changes in the paleoclimate (Wang et al., 2017a). Even though studies about dolomite in shales are abundant, the formation mechanism of dolomite found within shale remains inconclusive.

In this study we investigate a dolomite interlayer that is observed in late Ordovician black shale sediments of the Guanyinqiao Bed in Shizhu county, which is part of the upper Yangtze Block (SW China). It is an intriguing carbonate layer at the top of Wufeng Formation (end of Ordovician) normally consisting of shelly limestone and *Hirnantia-Dalmanitina* fauna fossils which was studied by many researchers (Ahm et al., 2017; Chen et al., 2001; Chen et al., 2017; Rong, 1979; Rong et al., 2002; Zhang et al., 2010). Besides the shelly limestone of the Guanyinqiao Bed, parts of the Bed are composed of dolomite at the margins of Sichuan Basin (Su, 2017; Zhou et al., 2017). Zhou et al. (2017) studied this dolomite in the Guanyinqiao Bed found in Bailu village (Wuxi

county) and suggested a primary origin of the dolomite as plenty of algae were observed under optical microscope. Ahm et al. (2017) also found a similar dolomite layer in corresponding strata called the Vinini Creek section in Nevada (USA) illustrating its global importance, however, these authors did not systematically study the formation of the dolomite.

In order to better understand the formation mechanism of dolomite found within shale, we applied carbonate clumped isotope thermometry to provide formation temperature estimates and applied in addition to that a wide suite of petrological and geochemical methods. The combined approach of these methods clearly revealed a hot diagenetic origin of these dolomite deposits.

2. Geological setting

The late Ordovician is a significant period in the geological history, during which the severe glaciation (Brenchley et al., 2003; Finnegan et al., 2011; Trotter et al., 2008) led to the fall of sea-level and not only resulted in the first Mass Extinction of Phanerozoic (Brenchley et al., 2003; Rong and Zhan, 1999) but also caused the Hirnantian isotopic carbon excursion (HICE) (Bergström et al., 2006, 2009, 2016; Chen et al., 2017; Delabroye and Vecoli, 2010; Edwards and Saltzman, 2016; Fan et al., 2009; Kump et al., 1999; Munnecke et al., 2011; Subías et al.,

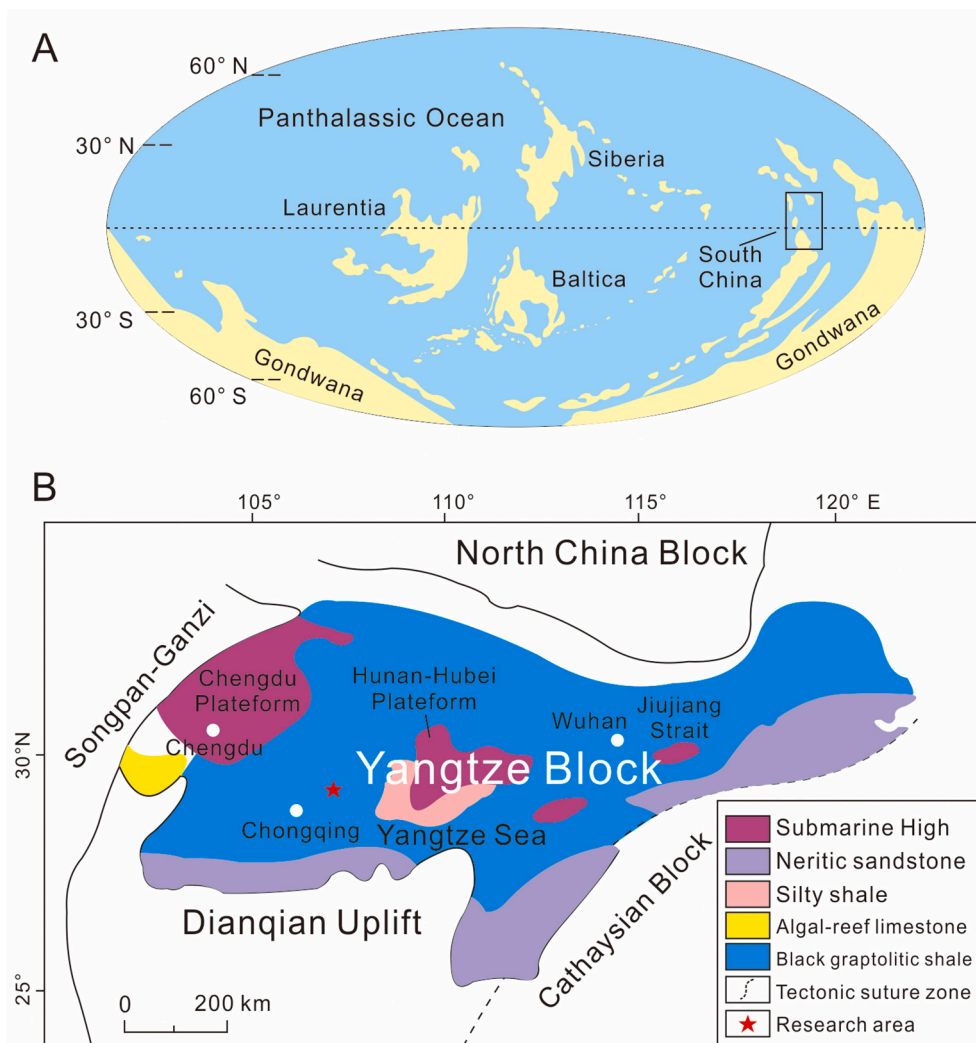


Fig. 1. Latest Ordovician palaeogeographic maps (A) (base map modified from (Zhou et al., 2015)) and blown up in (B) the Yangtze Block with our study area marked with a red star, modified from (Chen et al., 2004; Yan et al., 2010; Zhou et al., 2015). (For interpretation of the references to colour in this figure legend, the reader is referred to the web version of this article.)

2015; Tu et al., 2012; Wang et al., 1997). All of those geological phenomena were recorded by contemporary sediments and the strata deposited in upper Yangtze Block (SW China). The sediments covering the late Ordovician and early Silurian are part of the Wufeng and Longmaxi Formation (Chen et al., 2001; Rong, 1979; Rong et al., 2002), respectively. The dominant component of Wufeng Formation and Longmaxi Formation, black siliceous shale, are well studied (Wei et al., 2021; Xiong et al., 2015; Zhang et al., 2020; Zhao et al., 2017; Zhou et al., 2015).

During the late Ordovician the South China Craton was located at northwest of Gondwana (Fig. 1A) (Zhou et al., 2015) and the upper Yangtze Block developed in the southwest of China Craton that was mostly covered by Yangtze Sea (Wang, 1985). The carbonate sequence of Baota and Linxiang Formations and the clastic rocks of the Wufeng Formation were deposited successively (Yang et al., 2012) (Fig. 1B). To the south of the late Ordovician Yangtze Block were the Dianqian Uplift and Cathaysian Block (Chen et al., 2004; Yan et al., 2010; Zhou et al., 2015).

Numerous Ordovician-Silurian boundary (OSB) sections have been

studied in the Yangtze Block, among which the Wangjiawan north Section was designated as the Global Stratotype Section and Point (GSSP) (Chen et al., 2006). This Section is composed of the Wufeng Formation (late Ordovician) and Longmaxi Formation (early Silurian). The upper Wufeng Formation mainly consists of siliceous shale and the lower Longmaxi Formation is composed of shale, calcareous mudstone, and calcareous shale. At the top of the Wufeng Formation, there is a very thin layer composed of marl named Guanyinqiao Bed (Chen et al., 2001; Rong, 1979; Rong et al., 2002; Rong and Chen, 1987; Tu et al., 2012). In the upper Yangtze Block, the top of the Wufeng Formation deposited within the Hirnantian and generally consists of black siliceous shale, carbonate and tuff/bentonite interlayers (Nie et al., 2017; Zhao et al., 2016; Zhou et al., 2017). Shelly limestone and grainstone, sometimes with dark dolomite are commonly observed in the carbonate rocks of the Guanyinqiao Bed (Nie et al., 2017; Zhou et al., 2017). Generally the thickness of the carbonate strata is less than 10 m and *Hirnantia* Fauna fossils can be found (Chen et al., 2001; Rong, 1979; Rong et al., 2002; Rong and Chen, 1987). The Wufeng Formation and the overlying Longmaxi Formation, that deposited in early Silurian, is a continuous

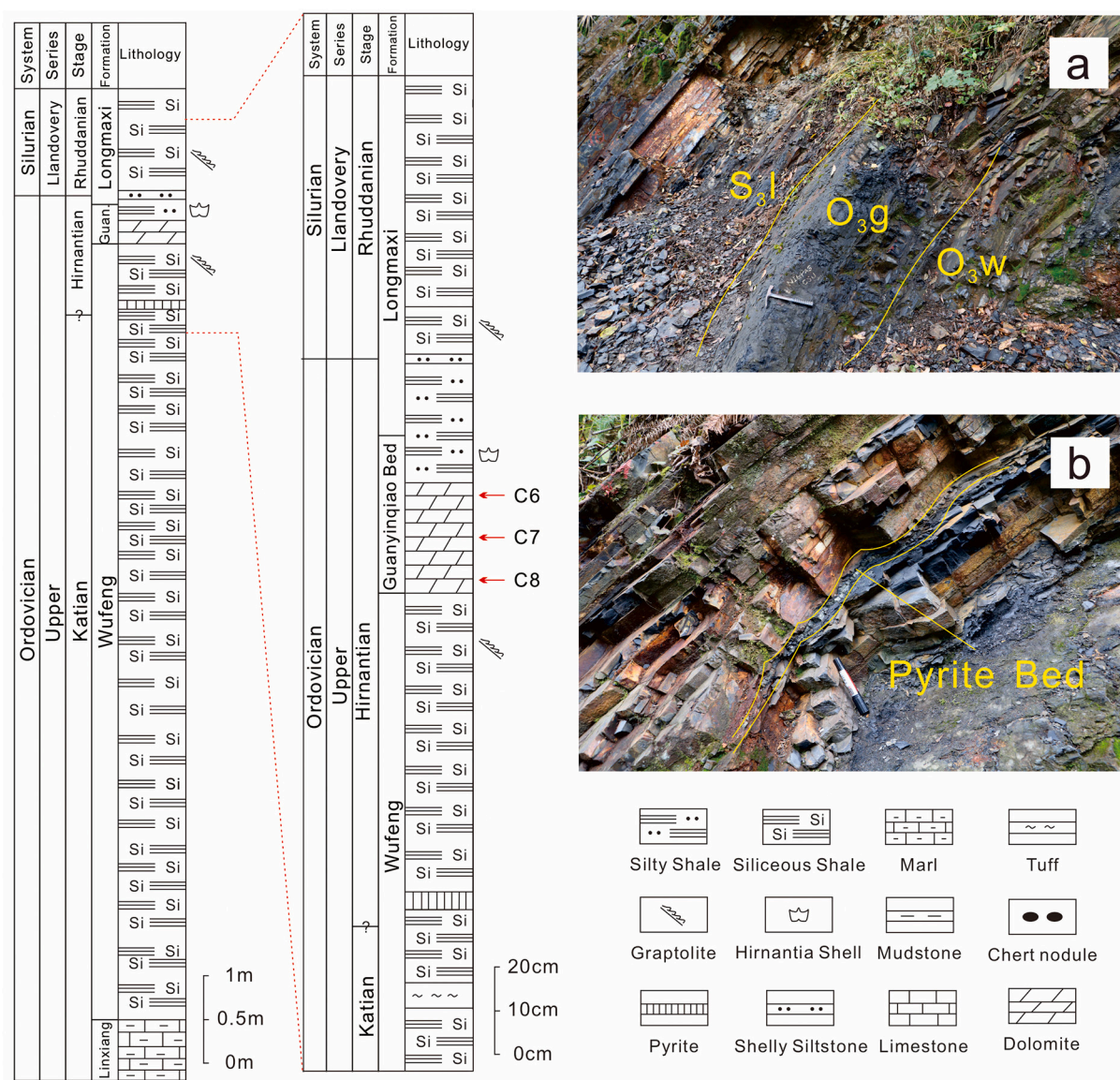


Fig. 2. Outcrop photos and lithology chart of Qiliao Section. The stratigraphic locations of the analyzed dolomite samples are indicated in the figure with the red arrows and their names (C6, C7 and C8). O₃w—Ordovician Wufeng Formation; O₃g—Ordovician Guanyinqiao Bed; S₃l—Silurian Longmaxi Formation. (For interpretation of the references to colour in this figure legend, the reader is referred to the web version of this article.)

contact (Chen et al., 2001; Rong, 1979; Rong et al., 2002).

Our study section at Shizhu county (Qiliao village) is located in the eastern Sichuan Basin (29°52'20"N, E 108°17'22"E), near the border of Chongqing Municipality and Hubei Province (Fig. 1-b). This area belongs to the transition zone of upper and middle Yangtze Platform and the OSB outcrop is situated at the southeast limb of Qiyueshan orogenic belt north part and the northwest limb of the Laochangping anticline (Fu, 2017). The successive sequence of the Linxiang, Wufeng and Longmaxi Formations are clearly observed in our study area (see Fig. 2). The Guanyinqiao Bed consists of black dolomite and siliceous shale is about 0.4 m thick and has a conformable contact with the overlying Longmaxi Formation (Fig. 2). The bottom part of upper Ordovician Wufeng Formation is comprised of black shale and a 2 cm thick pyrite bed about 0.6 m below the Guanyinqiao Bed (Fig. 2-B). The Guanyinqiao Bed consist of carbonate and the bottom of lower Longmaxi Formation Bed is comprised of black shale that is thought to be deposited simultaneously with a shallowing of sea level caused by the Hirnantian glaciation (Brenchley et al., 2003; Finnegan et al., 2011; Trotter et al., 2008) and the sediment environment changes from deep sea shelf to shallow sea shelf back to deep sea shelf (Nie et al., 2017; Zhao et al., 2016).

3. Sampling and methods

Unweathered siliceous shale from Wufeng and Longmaxi Formation and dolomite samples (C6, C7 and C8; see Fig. 2) were collected from Guanyinqiao Bed, respectively.

3.1. Petrological analyses

Samples were cut into pieces of 25 × 25 × 5 mm. One side of the thin sections was polished and cleaned in an ultrasonic bath. Then the polished side got glued on a glass slide, compressed and then placed in a dryer for 0.5 h. After that, cut and polished to 0.03mm thickness and put on a cover glass for petrographic observation. Petrographic observation was conducted with a LEICA-DMRX optical microscope and photomicrography taken with a LEICA-DC500. Microstructures of fresh rupture surfaces of carbonate samples were observed by Quanta 400 scanning electron microscope (SEM) and mineral crystals are confirmed by energy spectrum analysis. The degree of cation order of dolomite were analyzed by X-ray diffraction system D/MAX-III after the samples were grounded into powders with about 74 μm grainsize by agate mortar. The voltage was set at 40 kV and the electric current intensity was maintained at 40 mA. The results are calculated according to Füchtbauer and Goldschmidt (1966).

3.2. Geochemical analyses

The total organic carbon (TOC) contents were determined with help of LECO 200 carbon analyzer. Excess diluted hydrochloric acid (HCl) was used to remove the inorganic carbon and organic carbon was converted into CO₂ and CO based on the Dumas combustion method. Major elements were analyzed by X-ray fluorescence spectrometry (XRF1800) at the State Key Laboratory of Oil and Gas Reservoir Geology and Exploitation, Chengdu University of Technology, China. Analytical precision and accuracy for major elements are better than 4%. Trace elements were analyzed by ICP-AES & ICP-MS (Agilent 5110, 7900 and 7700x) at ALS Minerals-ALS Chemex (Guangzhou). Samples were divided into two portions. One portion was dissolved with HNO₃ + HClO₄ + HF + HCl and then dried samples were mixed with HCL and measured by ICP-AES and ICP-MS. Another portion was mixed with LiBO₂/Li₂B₄O₇ and melted in the oven ($T > 1025$ °C). When the temperature cooled down to the ambient temperature, HNO₃, HCL and HF were added and then measured by ICP-MS. Final results were selected according to the measured results. Standards are MRGEO08, OREAS-45e, OGGeo08, GBM908-10, STSD-1 and OREAS-120. The detection

limits for trace elements are ppb level and the errors are within 3%.

3.3. Isotope analyses

Carbon, oxygen and clumped isotope compositions were measured at the Department of Earth Sciences at Utrecht University with a Kiel IV carbonate device coupled to a Thermo Fisher Scientific MAT 253 isotope ratio mass spectrometer according to the methodology described in (Bernasconi et al., 2018; Meckler et al., 2014; Müller et al., 2019, 2017b; Schmid and Bernasconi, 2010). In general, for each measurement sequence (46 samples), 130 to 160 μg calcite standards (ETH-1, ETH-2 and ETH-3) and dolomite samples (QL-C6, QL-C7 and QL-C8) were weighed in glass vials and placed in the Kiel IV carbonate device. All samples (including calcite standards) were reacted with three drops of 103% phosphoric acid at 70 °C for 1300 s and the released CO₂ gas was continuously frozen away in a first liquid nitrogen trap (LN₂, −196 °C) of the Kiel device. When the reaction was finished, trap 1 was heated to −100 °C and the gas was transferred through a tube filled with 35 mm Porapak Type Q (50–80 mesh) embedded in silver wool into a second LN₂ trap. The Porapak trap was kept at −40 °C to remove potential contaminants such as halo-/hydrocarbons or reduced sulfur compounds. The phosphoric reaction time in our measurement sequences was 1300 s which is much longer than that in our normal calcite sample sequences. With longer reaction time we make certain to reach complete or near complete dolomite sample reaction (as dolomite reacts more sluggish with the acid) to avoid isotope fractionation. By using the same reaction time also for the calcitic standards in these measurement sequences we stick to the basic rule of equal standard sample treatment in stable isotope analyses. The samples were measured in the LIDI mode for 40 cycles with 10 s integration time, which gives 400 s in total for each sample or standard gas. Before starting the measurement sequence, pressure-sensitive baseline correction scans in the range of 25 to 5 V on m/z 44 were done to correct after the measurement sequence for the pressure dependence of the negative backgrounds (Bernasconi et al., 2013; Meckler et al., 2014; Müller et al., 2017a). Carbon and oxygen isotope composition of the carbonates are shown in delta notation relative to the Vienna Pee Dee Belemnite standard (VPDB) with parameters recommended by (Daëron et al., 2016). All results were presented as the mean values of replicates. We applied the $\delta^{18}\text{O}$ acid fractionation factor of 1.009926 for dolomite (Rosenbaum and Sheppard, 1986), the factor of 1.00871 for calcite standards (Kim and O'Neil, 1997) and conversion of VPDB scale into VSMOW scale was done by using $\delta^{18}\text{O}_{\text{SMOW}} = 1.03091 * \delta^{18}\text{O}_{\text{PDB}} + 30.91$ (Coplen et al., 1983). The oxygen and carbon isotopes of the samples were corrected using the accepted ETH calcite standard values (Bernasconi et al., 2018), the raw Δ_{47} values with the new accepted ETH calcite standard values in the I-CDES reference frame presented in Bernasconi et al. (2021) and the Δ_{47} temperatures of samples were calculated using the new Δ_{47} I-CDES 90 °C-temperature calibration of Anderson et al. (2021). Briefly described, we constructed an empirical transfer function (ETF) per measurement sequence from the background corrected raw Δ_{47} values and the new accepted Δ_{47} I-CDES 90 °C of the ETH standards for 90 °C reaction temperature and applied this ETF on the unknown dolomite samples to obtain the Δ_{47} I-CDES 90 °C in the absolute reference frame (Dennis et al., 2011). Due to the remaining uncertainties in the temperature dependent Δ_{47} acid fractionation correction for dolomite (Defliese et al., 2015; Müller et al., 2019, 2017b; Murray et al., 2016) and only limited dolomitic calibration samples in the new Δ_{47} I-CDES 90 °C-T calibration of Anderson et al. (2021), we additionally report in the supplementary data file results determined with old accepted ETH standard values (Bernasconi et al., 2018) and the dolomite specific Δ_{47} -temperature relationship for 70 °C acid reaction of Müller et al. (2019). We included the dolomitic check standards Sansa and Rodolo that can be received from the ETH clumped isotope laboratory, that are mentioned in Bernasconi et al. (2018) and Müller et al. (2019) for interlaboratory comparison. The new accepted ETH standards Δ_{47} I-CDES 90 °C were determined in a

recent inter laboratory comparison study by Bernasconi et al. (2021) involving multiple clumped isotope laboratories with various sample preparation approaches.

4. Results

4.1. Petrology and stratigraphy

The Wufeng Formation is approximately 8.8 m in thickness and the strata are dominated by siliceous shale. Tuff/bentonite beds, 0.01 to 0.1 m in thickness, occurred frequently from bottom to top (Fig. 2-A). A 2 cm thick pyrite bed about 0.6 m below the Guanyinqiao Bed appeared at the upper part of the Wufeng Formation (Fig. 2-B).

The Guanyinqiao Bed is about 0.4 m thick and composed of siliceous shale (Fig. 3-A) and dolomite (Fig. 3-B). The siliceous shale at the top of Guanyinqiao Bed is about 0.1 m thick and photomicrographs show that quartz is homogeneously distributed (Fig. 3-A), the dolomite bed is about 0.3 m thick and the dolomites are finely crystalized (Fig. 3-B). There are no fossils such as graptolites and other *Hirnantia* fauna present

in the Guanyinqiao Bed. With the help of scanning electron microscopy (SEM), the finely crystallized euhedral dolomite and clay minerals (Fig. 3-C) were visualized in selected samples of the Guanyinqiao Bed. Other than the Guanyinqiao Bed, dolomite was also found in silty shale samples from the strata above. The euhedral dolomite is smaller than that in Guanyinqiao Bed. Besides, bitumen and dolomite can be found in the cavity of radiolarian (Fig. 3-D and E). Abundant bioclastic debris can be found in the shelly siltstone (Fig. 3-F). Strata deposited at the final stage of Ordovician, that is overlying the Guanyinqiao Bed, are composed of shelly siltstone and silty shale. The thickness of the strata is about 0.15 m. The shelly siltstone at the top is considered as the boundary of Ordovician and Silurian (Mu et al., 1981; Rong, 1979; Zhou et al., 2017).

The Silurian strata are composed of black siliceous shale and the total thickness of the exposed strata is about 0.9 m. The black siliceous shale is similar to that in the Wufeng Formation.

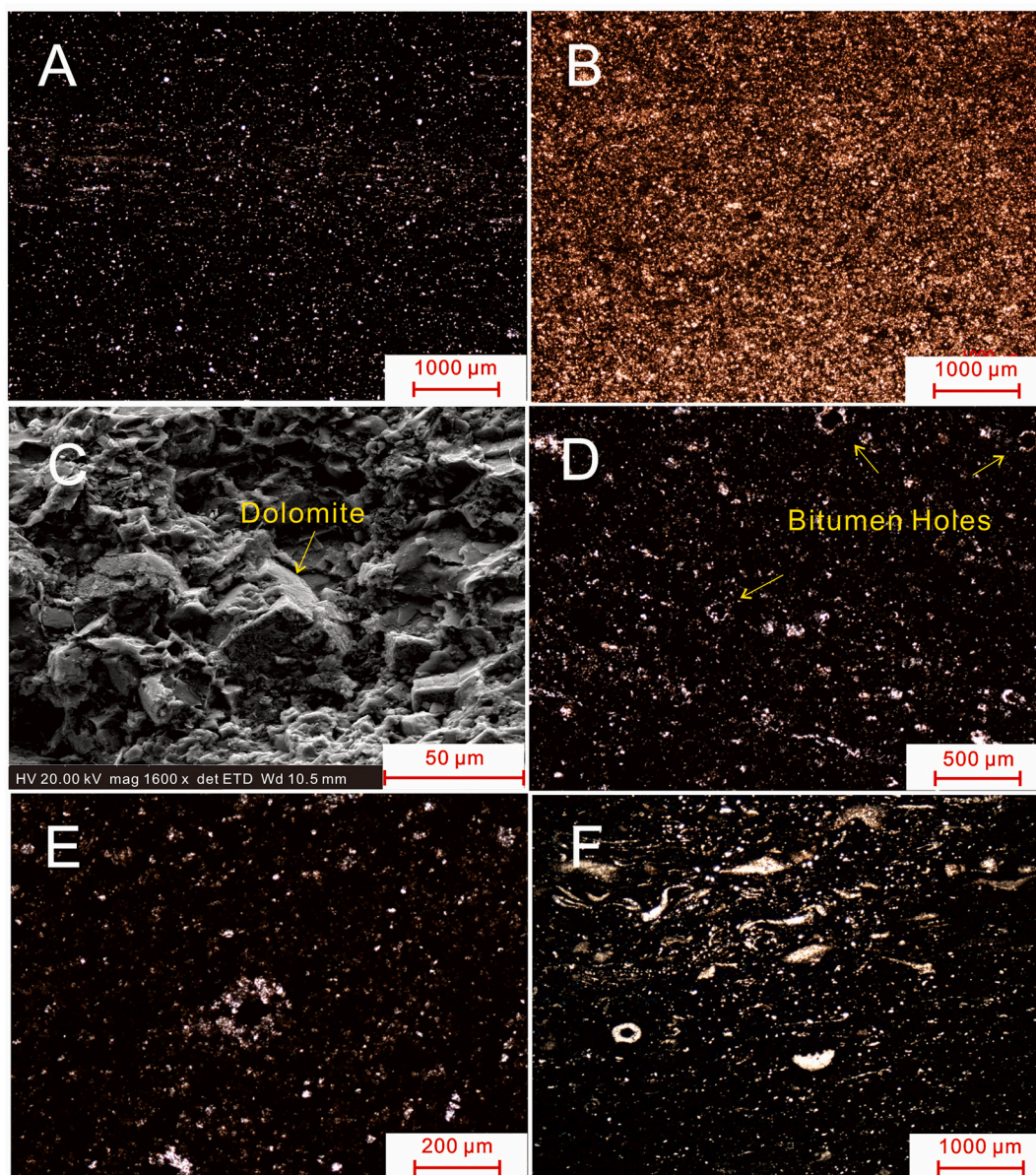


Fig. 3. Photomicrographs and scanning electron images of samples from Qiliao section. (A) Siliceous shale; (B) Guanyinqiao Bed Dolomite; (C) Dolomite observed under SEM; (D) Bitumen Holes in shale; (E) Dolomite in Bitumen Hole; (F) Shelly siltstone with bioclastic debris.

4.2. Cation ordering degree

Three dolomite samples were measured to determine the degree of cation order. Sample QL-C6 is from the top of the Guanyinqiao Bed, Mg and Ca contents are 47.33% and 52.67%, respectively, with the cation ordering degree of 0.39. Sample QL-C7 is from middle of the Guanyinqiao Bed, the contents of Mg and Ca are 47.43% and 52.57%, respectively, and the cation ordering degree is 0.39. Sample QL-C8 is from bottom of the Guanyinqiao Bed, Mg and Ca contents are 47.63% and 52.37%, respectively, with the cation ordering degree of 0.33 (Table 1). All of these three samples have the representative 101, 015 and 021 reflections (Fig. 4), which is indicative of well-ordered crystalline dolomite.

4.3. Total organic carbon

The TOC contents of samples from the top of the Guanyinqiao Bed (QL-C6-1 and QL-C6-2) are 3.86% and 3.75%, respectively. Samples from the middle (QL-C7-1 and QL-C7-2) have the TOC contents of 4.25% and 4.33%. And the TOC contents of that from the bottom (QL-C8-1 and QL-C8-2) are 3.80% and 3.69% (Table 2). The TOC contents of samples from the Longmaxi Formation (10.24 to 10.32%) and Wufeng Formation (8.23 to 8.31%) are much higher than that from Guanyinqiao Bed. All dolomite samples have a relative high content of organic carbon (>3%). Differences of the results from the various parts of the same sample partly reflect the analytical uncertainty and/or small differences due to carbon accumulation heterogeneity within the samples.

4.4. Major, trace and rare earth elements

The major, trace and rare earth elements (REEs) contents of 9 samples collected from the Guanyinqiao Bed were measured. The sample QL-C7-1 was not measured as it was destroyed when preparing the measurement. All of these samples have relatively high contents of Mn (2820 to 3540 µg/g) and are low in their Zn and Fe contents (12 to 64 µg/g and 2.64 to 3.99%, respectively) (Table 3). The contents of Sr and Th are low (223 to 279 µg/g and 2.72 to 4.80 µg/g, respectively) and Zr is relatively abundant (25.4 to 44.8 µg/g). The contents of REEs are depleted compared to Post-Archean Australian Shale (PAAS) (Taylor and McLennan, 1985) and LREEs are relatively enriched than HREEs (Table 4). The Eu/Eu* ratio (1.07 in average) shows minor positive anomaly and Ce/Ce* ratio (0.95 in average) shows slightly negative anomaly (Fig. 5).

4.5. Isotope analyses

The isotopic compositions of all individual measurements of samples and standards used for the data evaluation are displayed in the supplementary spreadsheet (sheet 1). Rejected measurements due to contamination, hardware issues or too small intensities due to incomplete reaction are marked in red in the table with all measurements. In the second sheet we only included the individual sample and dolomite check standard measurements that were used in this study. We included all replicates for the sample standards and calculated their average, standard deviation, 95% CI and number of individual analyses the averages are based on, these values are then used for Table 5. For the two dolomitic check standard analyses we obtained $\Delta_{47}^{\text{I-CDES } 90^\circ\text{C}}$ of $0.656 \pm$

0.023‰ for Rodolo based on 16 individual analyses and $0.544 \pm 0.051\text{‰}$ for Sansa based on only 9 individual analyses (for comparison to older studies the $\Delta_{47}^{\text{CDES } 70^\circ\text{C}}$ is $0.674 \pm 0.024\text{‰}$ for Rodolo and $0.555 \pm 0.055\text{‰}$ for Sansa, which were reported to be $0.632 \pm 0.006\text{‰}$ and $0.526 \pm 0.014\text{‰}$ in Müller et al., 2019, respectively). Compared to Rodolo and the unknown dolomite samples Sansa reacts very sluggish with phosphoric acid at our reaction temperature of 70°C and required additional grinding to finer grain size with pestle and mortar. In the first two measurement sequences we did not take this into account and obtained insufficient intensities due to incomplete reaction and did not use these first few analyses. In the later measurement sequences we grinded the Sansa powder before analyses and obtained higher yields with near complete reaction (we still observed visually some evolving gas bubbles, which was not the case for the unknown samples and Rodolo). Of the analyzed dolomite samples we report the averages with their uncertainties at the 95% confidence level and number of replicates in Table 5. The analyzed dolomite samples from the Guanyinqiao Bed have $\delta^{13}\text{C}_{\text{VPDB}}$ between $-3.17 \pm 0.04\text{‰}$ and $-2.48 \pm 0.03\text{‰}$ and $\delta^{18}\text{O}_{\text{VPDB}}$ between $-11.28 \pm 0.18\text{‰}$ to $-10.99 \pm 0.20\text{‰}$. The $\Delta_{47}^{\text{I-CDES } 90^\circ\text{C}}$ of the dolomite samples range from $0.418 \pm 0.027\text{‰}$ to $0.481 \pm 0.027\text{‰}$ (Table 5 and Fig. 6) resulting in temperatures of $73_{-14}^{+15}^\circ\text{C}$ for QL-C6, $112_{-18}^{+21}^\circ\text{C}$ for QL-C7 and $82_{-19}^{+23}^\circ\text{C}$ for QL-C8 (based on 17, 16 and 16 individual analyses, respectively). Evaluating the raw Δ_{47} with the old accepted standard values of Bernasconi et al. (2018) and using the dolomite specific temperature relation of Müller et al. (2019) resulted in average with 11°C colder $\Delta_{47}^{\text{CDES } 70^\circ\text{C}}$ -temperatures (see results marked in green in the supplementary data sheet). However, due to our large uncertainties and the lack of enough analyzed pure dolomites we use the results based on the novel accepted $\Delta_{47}^{\text{I-CDES } 90^\circ\text{C}}$ standard values of Bernasconi et al. (2021). The calculated $\delta^{18}\text{O}_{\text{w}}$ (VSMOW) of the fluid source using the oxygen isotope fractionation-temperature relationship of Horita (2014) ranges from $-3.7_{-2.4}^{+2.4}\text{‰}$ for QL-C6, $1.2_{-2.3}^{+2.3}\text{‰}$ for QL-C7 and $-2.6_{-3.1}^{+3.1}\text{‰}$ for QL-C8. Sample QL-C7 in the middle has slightly higher $\Delta_{47}^{\text{I-CDES } 90^\circ\text{C}}$ -temperature and positive $\delta^{18}\text{O}_{\text{w}}$ values than the samples above and below, but due to the beforementioned analytical challenges the estimates come with large uncertainty and are statistically indistinguishable.

5. Discussion

5.1. Formation temperature of dolomite

As the results shown in Table 1 and Fig. 4, well-ordered dolomite in our samples can be confirmed by X-ray diffraction (Fig. 4), although the cation ordering is not that high (0.33 to 0.39, Table 1) which maybe result from contamination of other minerals (probably Mg-silicates) as our samples are not pure dolomite. In our study we firstly study the formation conditions of this particular organic-rich dolomite layers in siliceous shale of the late Ordovician Guanyinqiao Bed with independent clumped isotope thermometry. Going down in the stratigraphic level of the studied dolomite interlayer and keeping in mind the distances between the samples is only about 10 cm we observed formation temperatures $73_{-14}^{+15}^\circ\text{C}$ for QL-C6, $112_{-18}^{+21}^\circ\text{C}$ for QL-C7 and $82_{-19}^{+23}^\circ\text{C}$ for QL-C8. Considering the large uncertainties in these Δ_{47} -T estimates due to the challenges of these impure and organic rich dolomites paired with a relatively low number of analyses (~16–17 individual measurements per sample), the obtained temperature differences are statistically not significant. That the dolomite interlayer formed under same conditions is further supported by the almost identical $\delta^{18}\text{O}_{\text{VPDB}}$ of the three dolomite samples with $-11.14 \pm 0.10\text{‰}$ (see supplementary file). Therefore, we constrained an overall formation temperature of the studied dolomite interlayer from Guanyinqiao Bed based on all 49 individual isotope analyses resulting in $87_{-10}^{+11}^\circ\text{C}$. In the following we will refer to this overall formation temperature estimate. The obtained formation temperature is clearly higher than the surface conditions in the upper Ordovician as during the deposition of the Guanyinqiao Bed

Table 1
Degree of cation order of Guanyinqiao dolomite.

Sample No.	Strata	Lithology	N(MgCO ₃ , %)	N(CaCO ₃ , %)	Degree of ordering
QL-C6	Guanyinqiao Bed	Dolomite	47.33	52.67	0.39
QL-C7		Dolomite	47.43	52.57	0.39
QL-C8		Dolomite	47.63	52.37	0.33

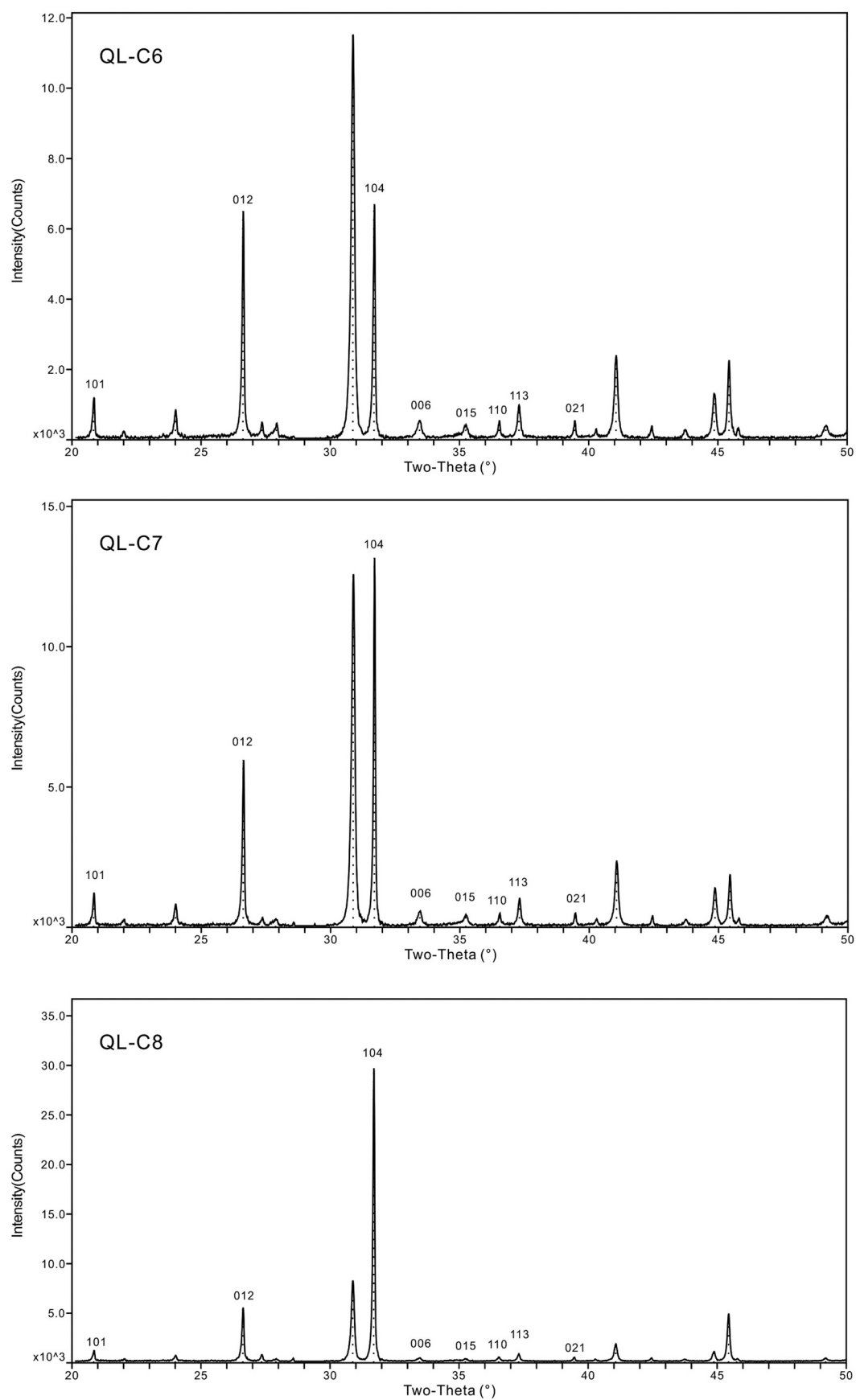


Fig. 4. X-ray diffraction pattern of the dolomite samples retrieved from the Guanyinqiao Bed with their 006, 015 and 110 ordering peaks well expressed.

Table 2

Total organic carbon content (wt, %) of samples from Guanyinqiao Bed.

Sample No.	Strata	Lithology	TOC
QL-C5-1	Longmaxi Formation	Shale	10.32
QL-C5-2			10.24
QL-C6-1	Guanyinqiao Bed	Dolomite	3.86
QL-C6-2			3.75
QL-C7-1			4.25
QL-C7-2			4.33
QL-C8-1	Wufeng Formation	Shale	3.80
QL-C8-2			3.69
QL-C9-1			8.23
QL-C9-2			8.31

the earth was undergoing a global glaciation event (Brenchley et al., 2003; Finnegan et al., 2011; Trotter et al., 2008) and primary dolomite precipitation in a shallow seawater environment can be ruled out. Comparing to the burial temperature gradient of surrounding drill cores from contemporary limestone strata (Luo et al., 2017), the depth of strata deposited during Hirnantian is around 2500 to 3000 m deep, which equals an approximate burial temperature of 75 to 90 °C. This burial agrees well with our novel Δ_{47} temperature estimate and is clear evidence that this dolomite interlayer formed at a later stage during burial.

With increasing burial depth pressure and temperature increases due to the overlying pressure and the geothermal gradient. In case these temperature conditions become too extreme, carbonate minerals are prone to solid-state reordering, an mineral internal isotope exchange process at the high ambient temperature (Dennis et al., 2011; Passey and Henkes, 2012). This process could potentially reset the Δ_{47} values of calcite/aragonite originally formed in the seawater and re-equilibrate them to the new conditions of burial depth while the carbon and oxygen isotope composition retains the original one (Lloyd et al., 2017). However, studies on solid state reordering on dolomite such as the one by Lloyd et al. (2018) suggest much higher temperature to trigger solid state reordering in dolomite. From the estimated maximum burial depths of less than 3000 m and expected temperatures around 90 °C it is very implausible that our studied dolomites were significantly affected by solid state reordering since the time the mineral formed. We thus expect that the Δ_{47} of the analyzed dolomites reflect the original formation temperature out of a diagenetic fluid in a former burial depth of approximately 3 km.

5.2. Properties of dolomitization fluid

In order to get a more complete picture of the genesis of our analyzed dolomite layer from the Guanyinqiao Bed, the fluid source in which the dolomite formed is crucial to know. With the obtained temperature estimates and simultaneously measured oxygen isotope composition of the dolomites, we calculated the $\delta^{18}\text{O}_w$ of the fluid source using the temperature dependent oxygen isotope fractionation relation between the dolomite and water of Horita (2014). Existing studies on the temperature relation of the oxygen isotope fractionation between dolomite and water were constructed for dolomites and/or proto-dolomites that

formed at different temperature ranges and the studies seem to show slight differences (Horita, 2014; Matthews and Katz, 1977). These differences and remaining uncertainties on the oxygen isotope fractionation were thoroughly discussed in Murray and Swart (2017) and we are aware that small uncertainties still exist in these fractionation factors. As the obtained Δ_{47} temperatures of our study are within the calibration temperature range of the most recent study by Horita (2014), based on calibration samples formed between 80 and 350 °C, which is ideal for our studied dolomites we decided to apply this one to constrain the presumable dolomite forming fluid source.

The calculated $\delta^{18}\text{O}_w$ (VSMOW) obtained from our dolomite samples going downward in the stratigraphical level are $-3.7_{-2.4}^{+2.4}$ ‰ for QL-C6, $1.2_{-2.3}^{+2.3}$ ‰ for QL-C7 and $-2.6_{-3.1}^{+3.1}$ ‰ for QL-C8. The large uncertainties at the 95% CI reflect mainly the large uncertainties in their temperature constraints (Fig. 6). The sample from the middle of the Guanyinqiao Bed (QL-C7) seems to have a $\delta^{18}\text{O}_w$ more positive than the others and the one from the top (QL-C6) has the most negative $\delta^{18}\text{O}_w$ value, however, the calculated values have a large uncertainty and are statistically indistinguishable. As the $\delta^{18}\text{O}_{\text{VPDB}}$ and the observed temperature range of the three dolomites is within their uncertainty, we also calculated the averaged $\delta^{18}\text{O}_w$ value of $-1.8_{-1.5}^{+1.5}$ ‰ (VSMOW) based on the average temperature of 87_{-10}^{+11} °C of all 49 individual analyses. Our obtained $\delta^{18}\text{O}_w$ value is in the range of estimates for late Ordovician seawater with reported $\delta^{18}\text{O}$ values of approximately -3‰ to -1‰ (Came et al., 2017; Cummins et al., 2014; Henkes et al., 2018; Qin and Veizer, 1994; Ryb and Eiler, 2018; Wallmann, 2001). The obtained temperature of 87_{-10}^{+11} °C is well in line with burial depth estimates and the slightly depleted $\delta^{18}\text{O}$ (-11.14‰) with respect to contemporary deposited limestone (-10‰) (Tu et al., 2012) give strong evidence that these dolomite layer precipitated out of a diagenetically altered fluid source.

Although we did not observe direct field evidence for magmatic activity in our study area, another potential fluid source with elevated temperature and heavy $\delta^{18}\text{O}_w$ could potentially originate from nearby magmatic activity. During middle Permian, the orogenic activity in southwest China was intense and resulted in the large magmatic activity which formed the Emeishan large igneous province (Fan et al., 2009; He et al., 2002; Huang et al., 1991). The range of this magmatic activity is very wide and Chongqing province, our study site is located in the outer part of the magmatic activity (He et al., 2002). Our calculated $\delta^{18}\text{O}_w$ range could be explained by a circulating hydrothermal fluid driven by this magmatic activity (Hoefs, 2009). Such hydrothermal fluids with similar temperature range and promoting dolomite formation in northern Italy, were shown to have relatively high Fe, Zn and Mn concentration (Carmichael and Ferry, 2008; Ferry et al., 2011). The Mn contents of dolomite samples from the Guanyinqiao Bed are also very high with 2820 to 3540 ppm, however, the content of Fe (2.64 to 3.99%), Mg (6.86 to 8.07%) and Zn (15 to 64 ppm) are extremely low. And in contrast to our study site, the site in northern Italy shows direct evidence of magmatic dikes in close proximity to the dolomite bodies.

In addition to our stable isotope analyses we analyzed the REE content of the dolomite layer to get further insights on the fluid source. The LREEs content of all samples from the Guanyinqiao Bed is relatively depleted and the content of HREEs is relatively enriched (Fig. 5). In

Table 3

Major (%) and trace elements contents (µg/g) of Guanyinqiao Bed samples.

Samples	Al (%)	Ca (%)	Fe (%)	K (%)	Mg (%)	Mn (µg/g)	Na (%)	S (%)	Sr (µg/g)	Th (µg/g)	Zn (µg/g)	Zr (µg/g)
QL-C6-1	1.26	14.70	2.90	0.51	7.21	3070	2.39	0.21	245	3.47	15	34.5
QL-C6-2	1.10	16.15	2.66	0.44	7.75	3540	0.71	0.08	279	2.72	31	25.4
QL-C6-3	1.16	15.65	2.64	0.44	7.77	3230	0.26	0.18	264	3.00	19	29.4
QL-C7-2	1.07	15.70	3.08	0.43	7.64	2950	0.22	0.07	268	2.75	64	28.3
QL-C7-3	1.05	15.30	2.72	0.41	7.59	2820	1.89	0.08	261	4.80	47	44.8
QL-C8-1	1.05	16.40	2.75	0.42	8.07	2940	0.19	0.10	274	3.18	12	29.8
QL-C8-2	1.76	13.85	3.99	0.75	6.86	2890	0.26	0.23	223	2.79	49	26.4
QL-C8-3	1.29	15.10	3.26	0.54	7.51	2940	0.21	0.32	251	3.54	44	33.3

Table 4
Rare earth elements contents ($\mu\text{g/g}$) of Guanyinqiao Bed samples.

Sample No.	La	Ce	Pr	Nd	Sm	Eu	Gd	Tb	Dy	Ho	Er	Tm	Yb	Lu	LREE	HREE	ΣREE	$\Sigma\text{LREE}/\Sigma\text{HREE}$	Eu/ Eu*	Ce/ Ce*	(Nd/ Yb) _n	(Dy/ Yb) _n	(La/ Yb) _n	Er/ Nd
QL-C6-1	10.8	21.50	2.40	10.0	2.24	0.53	2.35	0.35	2.05	0.47	1.30	0.19	1.23	0.18	47.47	8.12	55.59	5.85	1.09	0.99	0.68	1.00	0.65	0.13
QL-C6-2	9.1	16.50	1.95	8.0	1.82	0.47	2.02	0.29	1.67	0.35	1.01	0.15	0.95	0.16	37.84	6.60	44.44	5.73	1.15	0.92	0.70	1.06	0.71	0.13
QL-C6-3	10.0	19.80	2.34	9.4	2.15	0.49	2.24	0.33	1.87	0.40	1.12	0.16	1.06	0.18	44.18	7.36	51.54	6.00	1.05	0.96	0.74	1.06	0.70	0.12
QL-C7-1	10.4	18.20	2.00	8.4	1.98	0.51	2.21	0.34	1.93	0.41	1.13	0.18	1.15	0.16	41.49	7.51	49.00	5.52	1.15	0.93	0.61	1.01	0.67	0.13
QL-C7-2	10.6	19.90	2.39	11.4	2.98	0.67	3.67	0.58	3.15	0.63	1.63	0.23	1.52	0.23	47.94	11.64	59.58	4.12	0.95	0.92	0.62	1.25	0.51	0.14
QL-C8-1	8.0	15.30	1.72	7.1	1.64	0.43	1.74	0.31	1.57	0.34	0.92	0.14	0.90	0.14	34.19	6.06	40.25	5.64	1.20	0.96	0.66	1.05	0.66	0.13
QL-C8-2	15.5	30.50	3.37	13.7	3.18	0.64	3.22	0.48	2.81	0.59	1.73	0.26	1.70	0.27	66.89	11.06	77.95	6.05	0.94	0.99	0.67	1.00	0.67	0.13
QL-C8-3	11.2	21.30	2.62	11.7	3.11	0.75	3.89	0.57	3.28	0.65	1.81	0.26	1.77	0.25	50.68	12.48	63.16	4.06	1.02	0.92	0.55	1.12	0.47	0.15
Average	10.7	20.38	2.35	9.96	2.39	0.56	2.67	0.41	2.29	0.48	1.33	0.20	1.29	0.20	46.34	8.85	55.19	5.37	1.07	0.95	0.65	1.07	0.63	0.13
PAAS	38.2	78.6	8.83	33.9	5.55	1.08	4.66	0.77	4.68	0.99	2.85	0.41	2.82	0.43	166.16	17.61	183.77	9.44	0.21	4.28	12.02	1.66	2.82	0.08

Note: $\text{Eu}/\text{Eu}^* = \text{Eu}_n/(\text{Sm}_n * \text{Gd}_n)^{0.5}$; $\text{Ce}/\text{Ce}^* = \text{Ce}_n/(\text{La}_n * \text{Pr}_n)^{0.5}$ (Bau and Dulski, 1996; Webb and Kamber, 2000); "n" stands for PAAS normalized value; Eu/Eu^* , Ce/Ce^* , $(\text{Nd}/\text{Yb})_n$, $(\text{Dy}/\text{Yb})_n$ and $(\text{La}/\text{Yb})_n$ values of PAAS are not normalized.

contrast, dolomite formed under hydrothermal environment has generally relatively high content of LREEs and low content of HREEs (Michard, 1989; Olivarez and Owen, 1991). Thus the results from our samples are not consistent with the characteristics of hydrothermal fluid properties. On the other side, Eu and Ce, widely used as indicators of temperature, show an apparent positive anomaly of Eu/Eu^* and negative anomaly of Ce/Ce^* in line with a hydrothermal fluid (Bau, 1991; Bau and Dulski, 1996; Frimmel, 2009; German and Elderfield, 1990; Sverjensky, 1984; Tostevin et al., 2016). However, the dimension of the Eu/Eu^* and Ce/Ce^* determined in our samples (1.07 and 0.95, respectively) is very small compared to a hydrothermal fluid source. Because of these and the absence of direct magmatic activity observed in our field area, a hydrothermal fluid from the Emeishan magmatic activity seems implausible.

Moreover, rare earth elements such as Nd, Yb, Dy, Yb, and Er can be used as indicators to distinguish formation condition of shallow-marine environment. Compared to primary carbonates formed in shallow-marine environment with reported $(\text{Nd}/\text{Yb})_n$ ratio of 1.51 and $(\text{Dy}/\text{Yb})_n$ ratio of 1.25 (Madhavaraju and Ramasamy, 1999), our dolomite samples from Guanyinqiao Bed have smaller average ratios of 0.65 and 1.07, respectively. Besides, the Er/Nd ratio we obtained (0.13 in average) is significantly lower than normal seawater (about 0.27) (de Baar et al., 1988). This can be caused by diagenesis and/or input of detrital materials to less than 0.1 (de Baar et al., 1988). However, our $(\text{La}/\text{Yb})_n$ ratios (0.63 in average) is much lower than terrigenous particulate matter (1.30; Sholkovitz, 1990) which excludes detrital material input as important source for our samples. Furthermore, contamination of REE patterns by terrestrial particulate matter can be assessed by considering the relation of Th and Zr content with respect to the total REE content, as these two elements are enriched in detrital minerals (Frimmel, 2009). As shown in Fig. 7, Th and Zr show poor correlation with REE contents and suggest no contamination of REE patterns and limited input of terrestrial particulate matters. Considering all these observations we suggest that the source of the dolomitization fluid was a diagenetic fluid.

To further promote the ideal conditions for dolomite formation, the supply of additional Mg ions is crucial. A potential Mg source in our study area is the clay minerals of surrounding black shale layers. The illitization of clay minerals in deep buried anoxic and hot environment will release abundant Mg^{2+} (Boles and Franks, 1979; Kahle, 1965). Especially clay minerals from the smectite group contain Mg^{2+} . It was shown in laboratory experiments that smectite minerals are prone to illitization already at 50°C and start to release Mg^{2+} during this process (Drief et al., 2002). The clay found in the surrounding shale could have potentially supplied the diagenetic fluid with enough Mg^{2+} to form dolomite.

In the southwest and southeast of Sichuan basin, the Guanyinqiao Beds are widely spread whereas dolomite is rarely found in other sections. According to the extent of the Wufeng Formation on a paleogeographic map (Mou et al., 2014; Yang et al., 2012), dolomite precursor limestone formed on the continental shelf, but probably below the wave base and not in shallow-water environment. From our newly obtained clumped isotope temperature estimates of the Guanyinqiao bed dolomite of $87_{-10}^{+11}^\circ\text{C}$ we can now clearly demonstrate its diagenetic origin in line with existing burial depth temperature estimates from surrounding drill cores from contemporary limestone strata of Luo et al. (2017).

5.3. Potential formation mechanisms of organic-rich dolomites in black shales

Black shale usually forms in organic-rich environment which can provide CO_3^{2-} to help dolomite formation (Davies et al., 1991; Mansfield, 1980). Besides, the reducing environment that deposit black shale is also favorable to form dolomite (Machel and Mountjoy, 1986). Furthermore, the middle to deep stable water column can also form a

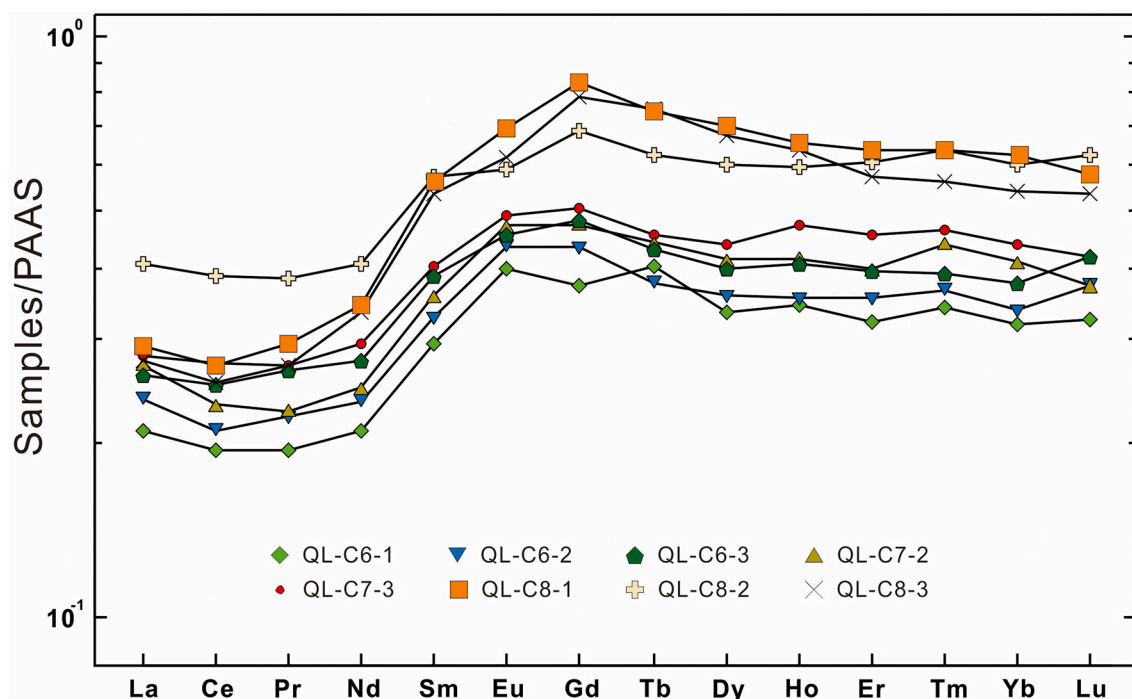


Fig. 5. PAAS-normalized REE diagram of Guanyinqiao Bed dolomite.

*Whole rock REE values were normalized against PAAS composition from (Taylor and McLennan, 1985).

Table 5

Stable and clumped isotope results of Guanyinqiao Bed dolomite.

Sample number	Numbers of replicates	$\delta^{13}\text{C}$ (‰, VPDB)	$\delta^{18}\text{O}$ (‰, VPDB)	Δ_{47} L-CDES 90 °C (‰)	T (°C)	$\delta^{18}\text{O}_w$ (‰, VSMOW)
QL-C6	17	-3.00 ± 0.04	-10.99 ± 0.20	0.481 ± 0.027	73_{-14}^{+15}	$-3.7_{-2.4}^{+2.4}$
QL-C7	16	-3.17 ± 0.04	-11.15 ± 0.13	0.418 ± 0.027	112_{-18}^{+21}	$1.2_{-2.3}^{+2.3}$
QL-C8	16	-2.48 ± 0.03	-11.28 ± 0.18	0.463 ± 0.036	82_{-19}^{+23}	$-2.6_{-3.1}^{+3.1}$

All uncertainties are displayed at the 95% CI.

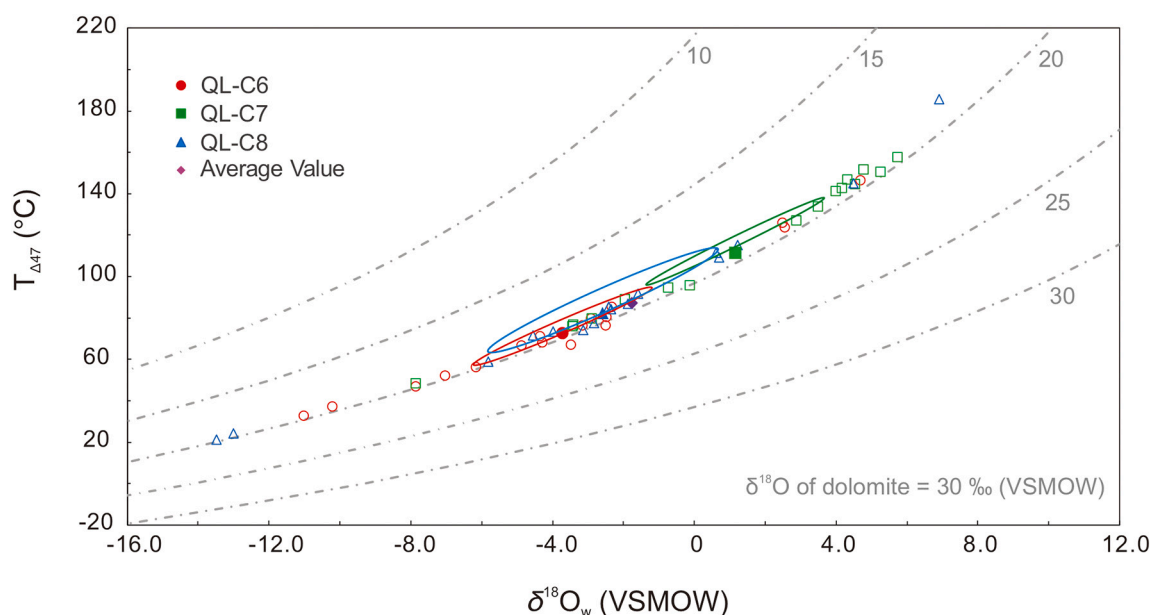


Fig. 6. Clumped isotope temperatures of the three dolomite samples from the Guanyinqiao Bed are plotted against their fluid source $\delta^{18}\text{O}_w$. Solid filled symbols stand for average values of each sample and unfilled symbols stand for all individual measurements of each sample. Dashed lines represent $\delta^{18}\text{O}$ of dolomite using temperature relationship of Horita (2014). Error bars of three samples are shown in error ellipses (95% CI). The offset between mean values of three samples and error ellipses centers is because the mean values are calculated from average Δ_{47} and error ellipses are based on individual temperature of each measurement.

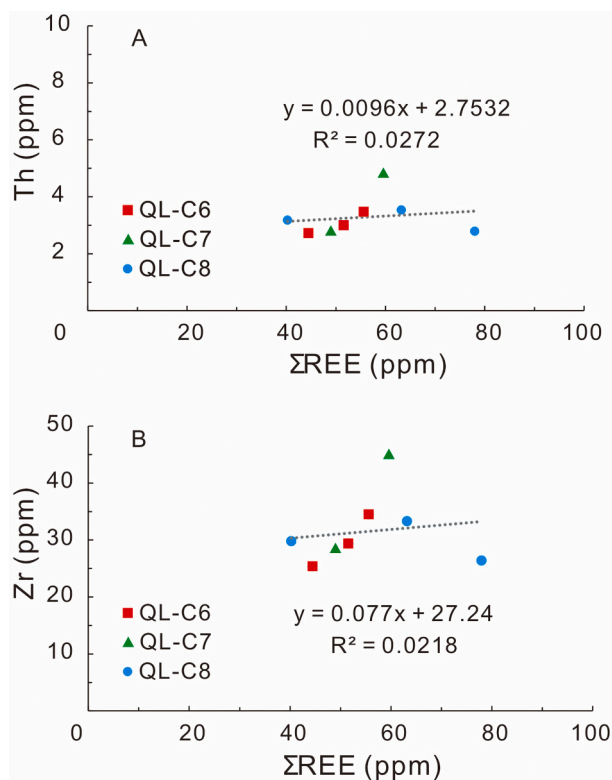


Fig. 7. Plot showing variation in Σ REE contents of all dolomite samples from Guanyinqiao Bed relative to (A) Th content and (B) Zr content.

high salinity environment that help the nucleation of dolomite (Liu et al., 2019; Wang et al., 2017b; Zhang, 1993). These factors would point on primary or early diagenetic dolomite formation mechanisms, which we can exclude now as important mechanisms for the dolomite layer of the Guanyinqiao Bed. Still, it is interesting to note that the analyzed dolomite samples from the Guanyinqiao Bed are also very enriched in organic matter and the TOC values are all higher than 3% (3.69 to 4.33%, Table 2), seen also in the black colour of our dolomite samples. The organic matter content in the black shale surrounding the dolomite layer is extremely high (8.23 to 10.32%) and the high content of organic matter found in the dolomites and black shales reflects the enhanced organic matter preservation under anoxic bottom water conditions and the diagenetic alteration from primary limestone to diagenetic dolomite preserved the organic matter.

Organic-rich dolomite not only occurs in Ordovician strata but also in the Permian Lucaogou Formation at Jungger Basin (Xinjiang) (Lei et al., 2012; Liu et al., 2019; Wang et al., 2017b; Zhang, 1993), the Proterozoic Doushantuo Formation at Hubei Province (Lan et al., 2019; Wang et al., 2017a; Wu et al., 2019). Furthermore, dolomite in shale is also found in the Wernecke Mountains Section in northwest of Canada of Ediacaran period (Ostrander et al., 2020), Marcellus shale in Monongalia county in U.S.A. of middle Devonian (Phan et al., 2019) and Silesian Basin in south Poland of Eocene to Oligocene (Bojanowski, 2014). This shows that organic-rich dolomite formed globally during different periods, more work on it needs to be done to better understand the potential role of organic matter in the dolomite formation and the Mg supply mechanism, but the findings of our study point on a late diagenetic origin.

6. Conclusion

In our study we demonstrate a hot diagenetic origin that formed the intriguing organic-rich dolomite layer of the Guanyinqiao Bed in black shales of the upper Ordovician Wufeng and the early Silurian Longmaxi

Formations. This time is known for widespread glaciation and low sea-level on Earth. In contrast to presumable cold primary formation conditions, our clumped isotope thermometry data reveal hot formation conditions of this particular organic-rich dolomite layer of 87_{-10}^{+11} °C based on 49 individual measurements on three samples. These high obtained formation temperatures are in line to burial depth estimates between 2500 and 3000 m in our study area. Together with REE signature we propose that the organic-rich dolomite layer formed from a hot diagenetic fluid source with a $\delta^{18}\text{O}_w$ of $-1.8_{-1.5}^{+1.5}$ ‰, which is similar to the presumable late Ordovician seawater composition. These elevated temperature conditions must have been ideal to release the required Mg^{2+} for the conversion of primary marine limestone to dolomite via the illitization process of surrounding clay minerals.

Declaration of Competing Interest

None.

Acknowledgements

We would like to thank Arnold van Dijk, Anne van der Meer and Ilja Kocken from Utrecht University and Mingshi Feng and Miao Deng from Chengdu University of Technology for their help in the laboratory. We also appreciate the editors and reviewers for their instructive suggestions. This study is founded by Department of Science and Technology of Sichuan Province, China (Grant No. 2021YJ0353) and NSF grants (Grant No. 41572085) of the Chinese Ministry of Science and Technology. Martin Ziegler and Inigo Müller acknowledge support from project 016.161.365, which is financed by the Netherlands Organization for Scientific Research (NWO).

Appendix A. Supplementary data

Supplementary data to this article can be found online at <https://doi.org/10.1016/j.chemgeo.2021.120641>.

References

- Ahm, A.S.C., Bjerrum, C.J., Hammarlund, E.U., 2017. Disentangling the record of diagenesis, local redox conditions, and global seawater chemistry during the latest Ordovician glaciation. *Earth Planet. Sci. Lett.* 459, 145–156. <https://doi.org/10.1016/j.epsl.2016.09.049>.
- Anderson, N.T., Kelson, J.R., Kele, S., Daëron, M., Bonifacie, M., Horita, J., Mackey, T.J., John, C.M., Kluge, T., Petschnig, P., Jost, A.B., Huntington, K.W., Bernasconi, S.M., Bergmann, K.D., 2021. A unified clumped isotope thermometer calibration (0.5–1,100 °C) using carbonate-based standardization. *Geophys. Res. Lett.* 48. <https://doi.org/10.1029/2020GL092069>.
- Bau, M., 1991. Rare-earth element mobility during hydrothermal and metamorphic fluid-rock interaction and the significance of the oxidation state of europium. *Chem. Geol.* 93, 219–230. [https://doi.org/10.1016/0009-2541\(91\)90115-8](https://doi.org/10.1016/0009-2541(91)90115-8).
- Bau, M., Dulski, P., 1996. Distribution of yttrium and rare-earth elements in the Penge and Kuruman iron-formations, Transvaal Supergroup, South Africa. *Precambrian Res.* 79, 37–55. [https://doi.org/10.1016/0301-9268\(95\)00087-9](https://doi.org/10.1016/0301-9268(95)00087-9).
- Bergström, S.M., Finney, S.C., Xu, C., Goldman, D., Leslie, S.A., 2006. Three new Ordovician global stage names. *Lethaia* 39, 287–288. <https://doi.org/10.1080/00241160600847439>.
- Bergström, S.M., Chen, X., Gutiérrez-marco, J.C., Dronov, A., 2009. The new chronostratigraphic classification of the Ordovician System and its relations to major regional series and stages and to $\delta^{13}\text{C}$ chemostratigraphy. *Lethaia* 42, 97–107. <https://doi.org/10.1111/j.1502-3931.2008.00136.x>.
- Bergström, S.M., Eriksson, M.E., Schmitz, B., Young, S.A., Ahlberg, P., 2016. Upper Ordovician $\delta^{13}\text{C}_{\text{org}}$ chemostratigraphy, K-bentonite stratigraphy, and biostratigraphy in southern Scandinavia: a reappraisal. *Palaeogeogr. Palaeoclimatol. Palaeoecol.* 454, 175–188. <https://doi.org/10.1016/j.palaeo.2016.04.037>.
- Bernasconi, S.M., Hu, B., Wacker, U., Fiebig, J., Breitenbach, S.F.M., Rutz, T., 2013. Background effects on Faraday collectors in gas-source mass spectrometry and implications for clumped isotope measurements. *Rapid Commun. Mass Spectrom.* 27, 603–612. <https://doi.org/10.1002/rcm.6490>.
- Bernasconi, S.M., Müller, I.A., Bergmann, K.D., Breitenbach, S.F.M., Fernandez, A., Hodell, D.A., Jaggi, M., Meckler, A.N., Millan, I., Ziegler, M., 2018. Reducing uncertainties in carbonate clumped isotope analysis through consistent carbonate-based standardization. *Geochemistry, Geophys. Geosystems* 19, 2895–2914. <https://doi.org/10.1029/2017GC007385>.

- Bernasconi, S.M., Daëron, M., Bergmann, K.D., Bonifacie, M., Meckler, A.N., Affek, H.P., Anderson, N., Bajnai, D., Barkan, E., Beverly, E., Blamart, D., Burener, L., Calmels, D., Chaduteau, C., Clog, M., Davidheiser-Kroll, B., Davies, A., Dux, F., Eiler, J.M., Elliott, B., Fetrov, A.C., Fiebig, J., Goldberg, S., Hermoso, M., Huntington, K.W., Hyland, E., Ingalls, M., Jaggi, M., John, C.M., Jost, A.B., Katz, S., Kelson, J., Kluge, T., Kocken, I.J., Laskar, A., Leutert, T.J., Liang, D., Lucarelli, J., Mackey, T.J., Mangenot, X., Meinicke, N., Modestou, S.E., Müller, I.A., Murray, S., Neary, A., Packard, N., Passey, B.H., Pelletier, E., Petersen, S., Piasecki, A., Schauer, A., Snell, K.E., Swart, P.K., Tripathi, A., Upadhyay, D., Vennemann, T., Winkelstern, I., Yarian, D., Yoshida, N., Zhang, N., Ziegler, M., 2021. InterCarb: a community effort to improve inter-laboratory standardization of the carbonate clumped isotope thermometer using carbonate standards. *Geochim. Geophys. Geosyst.* 22 <https://doi.org/10.1029/2020GC009588> e2020GC009588.
- Bojanowski, M.J., 2014. Authigenic dolomites in the Eocene-Oligocene organic carbon-rich shales from the Polish Outer Carpathians: evidence of past gas production and possible gas hydrate formation in the Silesian basin. *Mar. Pet. Geol.* 51, 117–135. <https://doi.org/10.1016/j.marpetgeo.2013.12.001>.
- Boles, J.R., Franks, S.G., 1979. Clay diagenesis in Wilcox sandstones of Southwest Texas; implications of smectite diagenesis on sandstone cementation. *J. Sediment. Res.* 49, 55–70. <https://doi.org/10.1306/212F76BC-2B24-11D7-8648000102C1865D>.
- Brenchley, P.J., Carden, G.A., Hints, L., Kaljo, D., Marshall, J.D., Martma, T., Meidla, T., Nolvak, J., 2003. High-resolution stable isotope stratigraphy of Upper Ordovician sequences: constraints on the timing of bioevents and environmental changes associated with mass extinction and glaciation. *Bull. Geol. Soc. Am.* 115, 89–104. [https://doi.org/10.1130/0016-7606\(2003\)115<0089:HRSISO>2.0.CO;2](https://doi.org/10.1130/0016-7606(2003)115<0089:HRSISO>2.0.CO;2).
- Came, R.E., Azmy, K., Tripathi, A., Olanipekun, B.J., 2017. Comparison of clumped isotope signatures of dolomite cements to fluid inclusion thermometry in the temperature range of 73–176 °C. *Geochim. Cosmochim. Acta* 199, 31–47. <https://doi.org/10.1016/j.gca.2016.10.028>.
- Carmichael, S.K., Ferry, J.M., 2008. Formation of replacement dolomite in the Latemar carbonate buildup, Dolomites, northern Italy: part 2. Origin of the dolomitizing fluid and the amount and duration of fluid flow. *Am. J. Sci.* 308, 885–904. <https://doi.org/10.2475/08.2008.01>.
- Chen, X., Rong, J., Zhou, Z., Zhang, Y., Zhan, R., Liu, J., Fan, J., 2001. The Central Guizhou and Yichang uplifts, upper Yangtze region, between Ordovician and Silurian. *Chin. Sci. Bull.* 46, 1580–1584. <https://doi.org/10.1007/bf02900587>.
- Chen, X., Rong, J., Li, Y., Boucot, A.J., 2004. Facies patterns and geography of the Yangtze region, South China, through the Ordovician and Silurian transition. *Palaeogeogr. Palaeoclimatol. Palaeoecol.* 204, 353–372. [https://doi.org/10.1016/S0031-0182\(03\)00736-3](https://doi.org/10.1016/S0031-0182(03)00736-3).
- Chen, X., Rong, J., Fan, J., Zhan, R., Mitchell, C.E., Harper, D.A.T., Melchin, M.J., Peng, P., Finney, S.C., Wang, X., 2006. The Global Boundary Stratotype Section and Point (GSSP) for the base of the Hirnantian Stage (the uppermost of the Ordovician System). *Episodes* 29, 183–196. <https://doi.org/10.18814/epiugs/2006/v29i3/004>.
- Chen, C., Wang, J., Algeo, T.J., Wang, Z., Tu, S., Wang, G., Yang, J., 2017. Negative $\delta^{13}\text{C}_{\text{carb}}$ shifts in Upper Ordovician (Hirnantian) Guanyingjiao Bed of South China linked to diagenetic carbon fluxes. *Palaeogeogr. Palaeoclimatol. Palaeoecol.* 487, 430–446. <https://doi.org/10.1016/j.palaeo.2017.09.030>.
- Coplen, T.B., Kendall, C., Hopple, J., 1983. Comparison of stable isotope reference samples. *Nature* 302, 236–238. <https://doi.org/10.1038/302236a0>.
- Cummins, R.C., Finnegan, S., Fike, D.A., Eiler, J.M., Fischer, W.W., 2014. Carbonate clumped isotope constraints on Silurian ocean temperature and seawater $\delta^{18}\text{O}$. *Geochim. Cosmochim. Acta* 140, 241–258. <https://doi.org/10.1016/j.gca.2014.05.024>.
- Daëron, M., Blamart, D., Peral, M., Affek, H.P., 2016. Absolute isotopic abundance ratios and the accuracy of Δ_{47} measurements. *Chem. Geol.* 442, 83–96. <https://doi.org/10.1016/j.chemgeo.2016.08.014>.
- Davies, D.K., Bryant, W.R., Vessell, R.K., Burkett, P.J., 1991. Porosities, permeabilities, and microfabrics of Devonian shale. In: Bennett, R.H., Bryant, W.R., Hulbert, M.H., Chiou, W.A., Faas, R.W., Kasprovicz, J., Li, H., Lomenick, T., O'Brien, N.R., Pamukcu, S., Smart, P., Weaver, C.E., Yamamoto, T. (Eds.), *Microstructure of Fine-Grained Sediments*. Springer, New York, pp. 109–119. https://doi.org/10.1007/978-1-4612-4428-8_10.
- de Baar, H.J.W., German, C.R., Elderfield, H., van Gaans, P., 1988. Rare earth element distributions in anoxic waters of the Cariaco Trench. *Geochim. Cosmochim. Acta* 52, 1203–1219. [https://doi.org/10.1016/0016-7037\(88\)90275-X](https://doi.org/10.1016/0016-7037(88)90275-X).
- Defliese, W.F., Hren, M.T., Lohmann, K.C., 2015. Compositional and temperature effects of phosphoric acid fractionation on Δ_{47} analysis and implications for discrepant calibrations. *Chem. Geol.* 396, 51–60. <https://doi.org/10.1016/j.chemgeo.2014.12.018>.
- Delabroye, A., Vecoli, M., 2010. The end-Ordovician glaciation and the Hirnantian Stage: a global review and questions about Late Ordovician event stratigraphy. *Earth-Science Rev.* 98, 269–282. <https://doi.org/10.1016/j.earscirev.2009.10.010>.
- Dennis, K.J., Affek, H.P., Passey, B.H., Schrag, D.P., Eiler, J.M., 2011. Defining an absolute reference frame for “clumped” isotope studies of CO_2 . *Geochim. Cosmochim. Acta* 75, 7117–7131. <https://doi.org/10.1016/j.gca.2011.09.025>.
- Drief, A., Martinez-Ruiz, F., Nieto, F., Sanchez, N.V., 2002. Transmission electron microscopy evidence for experimental illitization of smectite in K-enriched seawater solution at 50 °C and basic pH. *Clay Clay Miner.* 50, 746–756. <https://doi.org/10.1346/000986002762090146>.
- Edwards, C.T., Saltzman, M.R., 2016. Paired carbon isotopic analysis of Ordovician bulk carbonate ($\delta^{13}\text{C}_{\text{carb}}$) and organic matter ($\delta^{13}\text{C}_{\text{org}}$) spanning the Great Ordovician Biodiversification Event. *Palaeogeogr. Palaeoclimatol. Palaeoecol.* 458, 102–117. <https://doi.org/10.1016/j.palaeo.2015.08.005>.
- Fan, J., Peng, P., Melchin, M.J., 2009. Carbon isotopes and event stratigraphy near the Ordovician-Silurian boundary, Yichang, South China. *Palaeogeogr. Palaeoclimatol. Palaeoecol.* 276, 160–169. <https://doi.org/10.1016/j.palaeo.2009.03.007>.
- Ferry, J.M., Passey, B.H., Vasconcelos, C., Eiler, J.M., 2011. Formation of dolomite at 40–80 °C in the Latemar carbonate buildup, Dolomite, Italy, from clumped isotope thermometry. *Geology* 39, 571–574. <https://doi.org/10.1130/G31845.1>.
- Finnegan, S., Bergmann, K., Eiler, J.M., Jones, D.S., Fike, D.A., Eisenman, I., Hughes, N. C., Tripathi, A.K., Fischer, W.W., 2011. The magnitude and duration of late Ordovician-early Silurian glaciation. *Science* 331 (80), 903–906. <https://doi.org/10.1126/science.1200803>.
- Frimmel, H.E., 2009. Trace element distribution in Neoproterozoic carbonates as palaeoenvironmental indicator. *Chem. Geol.* 258, 338–353. <https://doi.org/10.1016/j.chemgeo.2008.10.033>.
- Fu, C., 2017. Study on Reservoir Characteristics and Shale Gas Enrichment of Wufeng-longmaxi Formation Shale in Southeast Chongqing. PhD thesis. China University of Mining and Technology (in Chinese with English abstract).
- Füchtbauer, H., Goldschmidt, H., 1966. Beziehungen zwischen Calciumgehalt und Bildungsbedingungen der Dolomite. *Geol. Rundsch.* 55, 29–40. <https://doi.org/10.1007/BF01982953>.
- Gao, P., He, Z., Lash, G.G., Li, S., Zhang, R., 2020. Origin of chert nodules in the Ediacaran Doushantuo Formation black shale from Yangtze Block, South China. *Mar. Pet. Geol.* 114, 104227. <https://doi.org/10.1016/j.marpetgeo.2020.104227>.
- German, C.R., Elderfield, H., 1990. Application of the Ce anomaly as a paleoredox indicator: the ground rules. *Paleoceanography* 5, 823–833. <https://doi.org/10.1029/PA005i005p0823>.
- He, W., Wang, X., Bu, J., 2002. The Eustatic cycles and the depth of water mass of the latest Ordovician Wufengian in the Yangtze Basin. *Acta Sedimentol. Sin.* 20, 367–375 (in Chinese with English abstract). <https://doi.org/10.3969/j.issn.1000-0550.2002.03.002>.
- Henkes, G.A., Passey, B.H., Grossman, E.L., Shenton, B.J., Yancey, T.E., Pérez-Huerta, A., 2018. Temperature evolution and the oxygen isotope composition of Phanerozoic oceans from carbonate clumped isotope thermometry. *Earth Planet. Sci. Lett.* 490, 40–50. <https://doi.org/10.1016/j.epsl.2018.02.001>.
- Hoefs, J., 2009. Stable isotope geochemistry. In: *Stable Isotope Geochemistry*, Sixth edition. Springer Berlin Heidelberg. <https://doi.org/10.1007/978-3-540-70708-0>.
- Horita, J., 2014. Oxygen and carbon isotope fractionation in the system dolomite-water- CO_2 at elevated temperatures. *Geochim. Cosmochim. Acta* 129, 111–124. <https://doi.org/10.1016/j.gca.2013.12.027>.
- Huang, Zhicheng, Huang, Zhongjin, Chen, Z., 1991. Volcanic rock and radiolarian silicilith of Wufeng Formation in lower Yangtze region. *Acta Sedimentol. Sin.* 9, 1–15 (in Chinese with English abstract). <https://doi.org/10.14027/j.cnki.cjxb.1991.02.001>.
- Kahle, C.F., 1965. Possible roles of clay minerals in the formation of dolomite. *SEPM J. Sediment. Res.* 35, 448–453. <https://doi.org/10.1306/74d712a3-2b21-11d7-8648000102c1865d>.
- Kim, S.T., O'Neil, J.R., 1997. Equilibrium and nonequilibrium oxygen isotope effects in synthetic carbonates. *Geochim. Cosmochim. Acta* 61, 3461–3475. [https://doi.org/10.1016/S0016-7037\(97\)00169-5](https://doi.org/10.1016/S0016-7037(97)00169-5).
- Kump, L.R., Arthur, M.A., Patzkowsky, M.E., Gibbs, M.T., Pinkus, D.S., Sheehan, P.M., 1999. A weathering hypothesis for glaciation at high atmospheric pCO_2 during the Late Ordovician. *Palaeogeogr. Palaeoclimatol. Palaeoecol.* 152, 173–187. [https://doi.org/10.1016/S0031-0182\(99\)00046-2](https://doi.org/10.1016/S0031-0182(99)00046-2).
- Lan, Z., Sano, Y., Yahagi, T., Tanaka, K., Shirai, K., Papineau, D., Sawaki, Y., Ohno, T., Abe, M., Yang, H., Liu, H., Jiang, T., Wang, T., 2019. An integrated chemostratigraphic ($\delta^{13}\text{C}$ - $\delta^{18}\text{O}$, $\delta^{87}\text{Sr}$ - $\delta^{86}\text{Sr}$) study of the Doushantuo Formation in western Hubei Province, South China. *Precambrian Res.* 320, 232–252. <https://doi.org/10.1016/j.precamres.2018.10.018>.
- Lei, C., Li, H., Yang, R., Cheng, J., 2012. Lacustrine microbial dolomite of the Middle Permian Lucaogou Formation in Ürümqi, Xinjiang. *J. Palaeogeogr.* 14, 767–775 (in Chinese with English abstract). <https://doi.org/10.7605/gdxb.2012.06.008>.
- Liu, Y., Zhou, D., Jiao, X., Feng, Q., Zhou, X., 2019. A preliminary study on the relationship between deep-sourced materials and hydrocarbon generation in lacustrine source rocks: an example from the Permian black rock series in Jimusar sag, Junggar Basin. *J. Palaeogeogr.* 21, 983–998 (in Chinese with English abstract). <https://doi.org/10.7605/gdxb.2019.06.067>.
- Lloyd, M.K., Eiler, J.M., Nabelek, P.I., 2017. Clumped isotope thermometry of calcite and dolomite in a contact metamorphic environment. *Geochim. Cosmochim. Acta* 197, 323–344. <https://doi.org/10.1016/j.gca.2016.10.037>.
- Lloyd, M.K., Ryb, U., Eiler, J.M., 2018. Experimental calibration of clumped isotope reordering in dolomite. *Geochim. Cosmochim. Acta* 242, 1–20. <https://doi.org/10.1016/j.gca.2018.08.036>.
- Luo, C., Wang, R., Shi, X., Zhang, J., Wu, W., Zhao, S., Zhang, C., Yang, Y., 2017. Biostratigraphy of the Wufeng to Longmaxi Formation at well n11 of Changning shale gas field. *J. Stratigr.* 41, 142–152 (in Chinese with English abstract). <https://doi.org/10.19839/j.cnki.dcxz.2017.02.003>.
- Machel, H.G., Mountjoy, E.W., 1986. Chemistry and environments of dolomitization - a reappraisal. *Earth Sci. Rev.* 23, 175–222. [https://doi.org/10.1016/0012-8252\(86\)90017-6](https://doi.org/10.1016/0012-8252(86)90017-6).
- Madhavaraju, J., Ramasamy, S., 1999. Rare earth elements in limestones of Kallankurichchi formation of Ariyalur Group, Tiruchirapalli Cretaceous, Tamil Nadu. *Geol. Soc. India* 54, 291–301.
- Mansfield, C.F., 1980. A urolith of biogenic dolomite-another clue in the dolomite mystery. *Geochim. Cosmochim. Acta* 44, 829–839. [https://doi.org/10.1016/0016-7037\(80\)90264-1](https://doi.org/10.1016/0016-7037(80)90264-1).
- Matthews, A., Katz, A., 1977. Oxygen isotope fractionation during the dolomitization of calcium carbonate. *Geochim. Cosmochim. Acta* 41, 1431–1438. [https://doi.org/10.1016/0016-7037\(77\)90249-6](https://doi.org/10.1016/0016-7037(77)90249-6).

- Meckler, A.N., Ziegler, M., Millán, M.I., Breitenbach, S.F.M., Bernasconi, S.M., 2014. Long-term performance of the Kiel carbonate device with a new correction scheme for clumped isotope measurements. *Rapid Commun. Mass Spectrom.* 28, 1705–1715. <https://doi.org/10.1002/rcm.6949>.
- Michard, A., 1989. Rare earth element systematics in hydrothermal fluids. *Geochim. Cosmochim. Acta* 53, 745–750. [https://doi.org/10.1016/0016-7037\(89\)90017-3](https://doi.org/10.1016/0016-7037(89)90017-3).
- Mou, C., Ge, X., Xu, X., Zhou, K., Liang, W., Wang, X., 2014. Lithofacies palaeogeography of the Late Ordovician and its petroleum geological significance in Middle-Upper Yangtze Region. *J. Palaeogeogr.* 16, 427–440 (in Chinese with English abstract). <https://doi.org/10.7605/gdxb.2014.04.036>.
- Mu, E., Li, J., Ge, M., Chen, X., Ni, Y., Lin, R., 1981. Paleogeographic maps of the Late Ordovician in the Central China region and their explanation. *J. Stratigr.* 5, 165–170 (in Chinese with English abstract).
- Müller, I.A., Fernandez, A., Radke, J., van Dijk, J., Bowen, D., Schwieters, J., Bernasconi, S.M., 2017a. Carbonate clumped isotope analyses with the long-integration dual-inlet (LIDI) workflow: scratching at the lower sample weight boundaries. *Rapid Commun. Mass Spectrom.* 31, 1057–1066. <https://doi.org/10.1002/rcm.7878>.
- Müller, I.A., Violay, M.E.S., Storck, J.C., Fernandez, A., van Dijk, J., Madonna, C., Bernasconi, S.M., 2017b. Clumped isotope fractionation during phosphoric acid digestion of carbonates at 70 °C. *Chem. Geol.* 449, 1–14. <https://doi.org/10.1016/j.chemgeo.2016.11.030>.
- Müller, I.A., Rodriguez-Blanco, J.D., Storck, J.C., do Nascimento, G.S., Bontognali, T.R., Vasconcelos, C., Benning, L.G., Bernasconi, S.M., 2019. Calibration of the oxygen and clumped isotope thermometers for (proto-)dolomite based on synthetic and natural carbonates. *Chem. Geol.* 525, 1–17. <https://doi.org/10.1016/j.chemgeo.2019.07.014>.
- Munnecke, A., Zhang, Y., Liu, X., Cheng, J., 2011. Stable carbon isotope stratigraphy in the Ordovician of South China. *Palaeogeogr. Palaeoclimatol. Palaeoecol.* 307, 17–43. <https://doi.org/10.1016/j.palaeo.2011.04.015>.
- Murray, S.T., Swart, P.K., 2017. Evaluating formation fluid models and calibrations using clumped isotope paleothermometry on Bahamian dolomites. *Geochim. Cosmochim. Acta* 206, 73–93. <https://doi.org/10.1016/j.gca.2017.02.021>.
- Murray, S.T., Arienzo, M.M., Swart, P.K., 2016. Determining the Δ_{47} acid fractionation in dolomite. *Geochim. Cosmochim. Acta* 174, 42–53. <https://doi.org/10.1016/j.gca.2015.10.029>.
- Nie, H., Jin, Z., Ma, X., Liu, Z., Lin, T., Yang, Z., 2017. Graptolites zone and sedimentary characteristics of Upper Ordovician Wufeng Formation-Lower Silurian Longmaxi Formation in Sichuan Basin and its adjacent areas. *Acta Pet. Sin.* 38, 160–174 (in Chinese with English abstract). <https://doi.org/10.7623/syxb201702004>.
- Olivarez, A.M., Owen, R.M., 1991. The europium anomaly of seawater: implications for fluvial versus hydrothermal REE inputs to the oceans. *Chem. Geol.* 92, 317–328. [https://doi.org/10.1016/0009-2541\(91\)90076-4](https://doi.org/10.1016/0009-2541(91)90076-4).
- Ostrander, C.M., Sahoo, S.K., Kendall, B., Jiang, G., Planavsky, N.J., Lyons, T.W., Nielsen, S.G., Owens, J.D., Gordon, G.W., Romaniello, S.J., Anbar, A.D., 2019. Multiple negative molybdenum isotope excursions in the Doushantuo Formation (South China) fingerprint complex redox-related processes in the Ediacaran Nanhua Basin. *Geochim. Cosmochim. Acta* 261, 191–209. <https://doi.org/10.1016/j.gca.2019.07.016>.
- Ostrander, C.M., Owens, J.D., Nielsen, S.G., Lyons, T.W., Shu, Y., Chen, X., Sperling, E.A., Jiang, G., Johnston, D.T., Sahoo, S.K., Anbar, A.D., 2020. Thallium isotope ratios in shales from South China and northwestern Canada suggest widespread O₂ accumulation in marine bottom waters was an uncommon occurrence during the Ediacaran Period. *Chem. Geol.* 557, 119856. <https://doi.org/10.1016/j.chemgeo.2020.119856>.
- Passey, B.H., Henkes, G.A., 2012. Carbonate clumped isotope bond reordering and geospeedometry. *Earth Planet. Sci. Lett.* 351–352, 223–236. <https://doi.org/10.1016/j.epsl.2012.07.021>.
- Phan, T.T., Hakala, J.A., Lopano, C.L., Sharma, S., 2019. Rare earth elements and radiogenic strontium isotopes in carbonate minerals reveal diagenetic influence in shales and limestones in the Appalachian Basin. *Chem. Geol.* 509, 194–212. <https://doi.org/10.1016/j.chemgeo.2019.01.018>.
- Qin, H., Veizer, J., 1994. Oxygen and carbon isotopic composition of Ordovician brachiopods: Implications for coeval seawater. *Geochim. Cosmochim. Acta* 58, 4429–4442.
- Rong, J., 1979. The Hirnantia Fauna of China with the comments on the Ordovician-Silurian boundary. *J. Stratigr.* 3, 1–82 (in Chinese with English abstract).
- Rong, J., Chen, X., 1987. Faunal differentiation, biofacies and lithofacies pattern of late Ordovician (Ashgillian) in South China. *Acta Palaeontol. Sin.* 26, 507–535 (in Chinese with English abstract).
- Rong, J., Zhan, R., 1999. Ordovician-Silurian Brachiopod fauna turnover in South China. *Geoscience* 13, 390–394 (in Chinese with English abstract).
- Rong, J., Chen, X., Harper, D.A.T., 2002. The latest Ordovician Hirnantia Fauna (Brachiopoda) in time and space. *Lethaia* 35, 231–249. <https://doi.org/10.1111/j.1502-3931.2002.tb00081.x>.
- Rosenbaum, J., Sheppard, S.M.F., 1986. An isotopic study of siderites, dolomite and ankerites at high temperatures. *Geochim. Cosmochim. Acta* 50, 1147–1150. [https://doi.org/10.1016/0016-7037\(86\)90396-0](https://doi.org/10.1016/0016-7037(86)90396-0).
- Ryb, U., Eiler, J.M., 2018. Oxygen isotope composition of the Phanerozoic ocean and a possible solution to the dolomite problem. *Proc. Natl. Acad. Sci. U. S. A.* 115, 6602–6607. <https://doi.org/10.1073/pnas.1719681115>.
- Schmid, T.W., Bernasconi, S.M., 2010. An automated method for “clumped-isotope” measurements on small carbonate samples. *Rapid Commun. Mass Spectrom.* 24, 1955–1963. <https://doi.org/10.1002/rcm.4598>.
- Sholkovitz, E.R., 1990. Rare-earth elements in marine sediments and geochemical standards. *Chem. Geol.* 88, 333–347. [https://doi.org/10.1016/0009-2541\(90\)90097-Q](https://doi.org/10.1016/0009-2541(90)90097-Q).
- Su, X., 2017. Sedimentological and Geochemical Responses of Geological Events at the Ordovician-Silurian Boundary: The Example From Wufeng-Longmaxi Formations in Qiliiao Section, Shizhu. Master thesis. Chengdu University of Technology (in Chinese with English abstract).
- Subías, I., Villas, E., Álvaro, J.J., 2015. Hirnantian (Late Ordovician) $\delta^{13}\text{C}$ HICE excursion in a North Gondwanan (NE Spain) periglacial setting and its relationship to glacioeustatic fluctuations. *Chem. Erde* 75, 335–343. <https://doi.org/10.1016/j.chemer.2015.05.002>.
- Sverjensky, D.A., 1984. Europium redox equilibria in aqueous solution. *Earth Planet. Sci. Lett.* 67, 70–78. [https://doi.org/10.1016/0012-821X\(84\)90039-6](https://doi.org/10.1016/0012-821X(84)90039-6).
- Taylor, S.R., McLennan, S.M., 1985. *The Continental Crust: Its Composition and Evolution*. Blackwell Scientific Publications, Oxford.
- Tostevin, R., Shields, G.A., Tarbuck, G.M., He, T., Clarkson, M.O., Wood, R.A., 2016. Effective use of cerium anomalies as a redox proxy in carbonate-dominated marine settings. *Chem. Geol.* 438, 146–162.
- Trotter, J.A., Williams, I.S., Barnes, C.R., Lécuyer, C., Nicoll, R.S., 2008. Did cooling oceans trigger Ordovician biodiversification? Evidence from conodont thermometry. *Science* 321 (80), 550–554. <https://doi.org/10.1126/science.1155814>.
- Tu, S., Wang, Z., Wang, J.S., 2012. Interpretation for high resolution stable carbon and oxygen isotope records across Ordovician-Silurian boundary from Wangjiawan, South China. *Earth Sci. J. China Univ. Geosci.* 37, 165–174 (in Chinese with English abstract). <https://doi.org/10.3799/dqkx.2012.52.017>.
- Wallmann, K., 2001. The geological water cycle and the evolution of marine $\delta\text{O}18\text{O}$ values. *Geochim. Cosmochim. Acta* 65, 2469–2485. [https://doi.org/10.1016/S0016-7037\(01\)00603-2](https://doi.org/10.1016/S0016-7037(01)00603-2).
- Wang, H., 1985. *Atlas of the Palaeogeography of China*. Institute of Geology, Chinese Academy of Geological sciences, Wuhan College of Geology, Wuhan.
- Wang, K., Chatterton, B.D.E., Wang, Y., 1997. An organic carbon isotope record of late Ordovician to early Silurian marine sedimentary rocks, Yangtze Sea, South China: implications for CO₂ changes during the Hirnantian glaciation. *Palaeogeogr. Palaeoclimatol. Palaeoecol.* 132, 147–158. [https://doi.org/10.1016/S0031-0182\(97\)00046-1](https://doi.org/10.1016/S0031-0182(97)00046-1).
- Wang, Z., Wang, J., Suess, E., Wang, G., Chen, C., Xiao, S., 2017a. Silicified glendonites in the Ediacaran Doushantuo Formation (South China) and their potential paleoclimatic implications. *Geology* 45, 115–118. <https://doi.org/10.1130/G38613.1>.
- Wang, Y., Zhang, K., Lin, H., Chen, S., Zhang, G., Wang, Yuxin, 2017b. Controlling factors and model of mixed deposits of Lucaogou Formation on the periphery of Bogda Mountain. *Xinjiang. Pet. Geol.* 38, 686–692 (in Chinese with English abstract). <https://doi.org/10.7657/XJPG20170609>.
- Webb, G.E., Kamber, B.S., 2000. Rare earth elements in Holocene reefal microbialites: a new shallow seawater proxy. *Geochim. Cosmochim. Acta* 64, 1557–1565. [https://doi.org/10.1016/S0016-7037\(99\)00400-7](https://doi.org/10.1016/S0016-7037(99)00400-7).
- Wei, C., Dong, T., He, Z., He, S., He, Q., Yang, R., Guo, X., Hou, Y., 2021. Major, trace-elemental and sedimentological characterization of the upper Ordovician Wufeng-lower Silurian Longmaxi formations, Sichuan Basin, south China: insights into the effect of relative sea-level fluctuations on organic matter accumulation in shales. *Mar. Pet. Geol.* 126. <https://doi.org/10.1016/j.marpetgeo.2021.104905>.
- Wu, H., Jiang, S., Palmer, M.R., Wei, H., Yang, J., 2019. Positive cerium anomaly in the Doushantuo cap carbonates from the Yangtze platform, South China: implications for intermediate water column manganese conditions in the aftermath of the Marinoan glaciation. *Precambrian Res.* 320, 93–110. <https://doi.org/10.1016/j.precamres.2018.10.019>.
- Xiong, X., Wang, J., Yu, Q., Yang, Y., Xiong, G., Niu, B., Guo, X., Deng, Q., 2015. Element geochemistry inversion of the environment and background of organic-rich black shale formations: a case study of the Wufeng-Longmaxi black shale in the Tianba section in northeastern Chongqing. *Nat. Gas Ind.* 35, 25–32 (in Chinese with English abstract). <https://doi.org/10.3787/j.issn.1000-0976.2015.04.004>.
- Yan, D., Chen, D., Wang, Q., Wang, J., 2010. Large-scale climatic fluctuations in the latest Ordovician on the Yangtze block, South China. *Geology* 38, 599–602. <https://doi.org/10.1130/G30961.1>.
- Yang, W., Xie, W., Wei, G., Liu, M., Zeng, F., Xie, Z., Jin, H., 2012. Sequence lithofacies paleogeography, favorable reservoir distribution and exploration zones of the Cambrian and Ordovician in Sichuan Basin, China. *Acta Pet. Sin.* 33, 21–34 (in Chinese with English abstract). <https://doi.org/10.7623/syxb2012S2003>.
- Zhang, X., 1993. Study of the origin of the dolostone intercalated in the black shale in middle Permian Lucaogou Formation eastern part of southern margin of Jungar Basin. *Acta Sedimentol. Sin.* 11, 133–140 (in Chinese with English abstract). <https://doi.org/10.14027/j.cnki.cjxb.1993.02.018>.
- Zhang, R., Liu, J., Percival, I.G., Jin, J., Li, G., 2010. Biodiversification of Late Ordovician Hirnantia fauna on the Upper Yangtze Platform, South China. *Sci. China Earth Sci.* 53, 1800–1810 (in Chinese with English abstract). <https://doi.org/10.1007/s11430-010-4071-3>.
- Zhang, W., Hu, W., Borjigin, T., Zhu, F., 2020. Pore characteristics of different organic matter in black shale: a case study of the Wufeng-Longmaxi Formation in the Southeast Sichuan Basin, China. *Mar. Pet. Geol.* 111, 33–43. <https://doi.org/10.1016/j.marpetgeo.2019.08.010>.
- Zhao, J., Jin, Zhijun, Jin, Zhenkui, Wen, X., Geng, Y., Yan, C., Nie, H., 2016. Lithofacies types and sedimentary environment of shale in Wufeng-Longmaxi Formation, Sichuan Basin. *Acta Pet. Sin.* 37, 572–586 (in Chinese with English abstract). <https://doi.org/10.7623/syxb201605002>.
- Zhao, J., Jin, Zhijun, Jin, Zhenkui, Hu, Q., Hu, Z., Du, W., Yan, C., Geng, Y., 2017. Mineral types and organic matters of the Ordovician-Silurian Wufeng and Longmaxi

- Shale in the Sichuan Basin, China: implications for pore systems, diagenetic pathways, and reservoir quality in fine-grained sedimentary rocks. *Mar. Pet. Geol.* 86, 655–674. <https://doi.org/10.1016/j.marpetgeo.2017.06.031>.
- Zhou, L., Algeo, T.J., Shen, J., Hu, Z.F., Gong, H., Xie, S., Huang, J.H., Gao, S., 2015. Changes in marine productivity and redox conditions during the Late Ordovician Hirnantian glaciation. *Palaeogeogr. Palaeoclimatol. Palaeoecol.* 420, 223–234. <https://doi.org/10.1016/j.palaeo.2014.12.012>.
- Zhou, Y., Ding, J., Yu, Q., Wang, J., Men, Y., Xiong, G., Xiong, X., Deng, Q., 2017. Sedimentary and organic carbon isotopic characteristics of the Kuanyinchiao member in northeastern Chongqing and its regional correlation. *Acta Geol. Sin.* 91, 1097–1107 (in Chinese with English abstract).